HRV.Ox

Development and evaluation of a low-cost photoplethysmography sensor monitoring vital signs such as heart rate, heart rate variability and oxygen saturation.

Master Thesis

For attainment of the academic degree of
Master of Science in Engineering (MSc)

in the Master Programme Digital Healthcare
at St. Pölten University of Applied Sciences

by
Markus Paßecker
1510756826

First advisor: Andreas Jakl, MSc
Second advisor: FH-Prof. Jakob Doppler, MSc

Sankt Pölten, 17.01.2018

Declaration

I declare that I have developed and written the enclosed Master Thesis completely by myself, and have not used sources or means without declaration in the text. Any thoughts from others or literal quotations are clearly marked. This work was not used in the same or in a similar version to achieve an academic grading or is being published elsewhere.

....

Place, Date Signature

Abstract

Photoplethysmography (PPG) is a simple and low-cost optical technique which can be used to determine blood volume changes in the microvascular bed of tissue. This technique is based on the use of one light source and a light detector, operating in light transmission or reflection mode. This device allows to determine information on the cardiovascular system, and can be used to derive blood oxygen saturation measurements operating with red and infrared light.

The aim of this work is to test and compare the performance of a developed low-cost PPG prototype to current devices used for the detection of RR-intervals during heartbeat and blood oxygen saturation measurements, respectively Electrocardiography (ECG) and Pulse Oximeter.

Five subjects have been equipped with the above-mentioned devices and their data have been recorded for five minutes during “rest” and “moderate exertion” phases. The results of the measurements have been algorithmically processed and analysed in order to obtain the variables of interest, namely the RR-intervals and blood oxygen saturation. The tool selected for the interpretation of the results of RR-intervals measurements is the Bland-Altman plot.

ECG and PPG devices have shown a good agreement for datasets acquired during the rest phase. Nevertheless, the level of agreement decreases for datasets related to “moderate exertion” phases, probably because of motion artefacts which affect the operation of both devices. Pulse oximeter and PPG devices showed a moderate agreement, even though the measured values were within a reasonable range.

Further developments of the prototype, e.g. through acceleration based motion artefacts reduction, as well as clinical calibration might be considered to improve the performances of the device in both measurements, respectively RR-intervals and blood oxygen saturation.

Kurzfassung

Die Photoplethysmographie (PPG) ist eine einfache und kostengünstige optische Methode, mit der Volumenänderungen im mikrovaskulären Gewebe der Haut bestimmt werden können. Die Methode basiert auf der Verwendung einer Lichtquelle und einem Lichtdetektor, wobei von der Haut reflektiertes oder absorbiertes Licht gemessen wird. Dadurch können sowohl Informationen über das Herz-Kreislauf-System als auch über die Sauerstoffsättigung einer Person gewonnen werden.

Ziel dieser Arbeit ist der Untersuchung und Evaluation eines in dieser Arbeit entwickelten Prototypen zur Messung der Herzrate, der Herzratenvariabilität sowie der Sauerstoffsättigung. Die gemessenen Daten wurden mit dem goldenen Standard, der Elektrokardiographie sowie mit einem handelsüblichen Pulsoxymeters verglichen.

Fünf Testpersonen wurden mit den oben genannten Geräten ausgestattet und deren Körperwerte für fünf Minuten sowohl während einer Ruhephase als auch in einer Phase moderater körperlicher Belastung aufgezeichnet, algorithmisch analysiert und ausgewertet. Die berechneten RR-Intervalle als auch die Sauerstoffsättigung der Testpersonen wurde danach mithilfe des Bland-Altman-Diagramms interpretiert.

Die evaluierten Daten des entwickelten PPG-Prototypen verglichen mit denen des ECG Gerätes führten zu einer guten Übereinstimmung in Ruhephasen der Testpersonen. Aufgrund von Bewegungsartefakten sank in Phasen der moderaten körperlichen Anstrengung die Übereinstimmung. Beim Vergleich der Sauerstoffsättigung der Probanden und Probandinnen konnte moderate Übereinstimmung mit dem handelsüblichen Fingerpulsoxymeters erzielt werden.

Für zukünftige Weiterentwicklungen des Prototyps, sollten Verbesserungen, beispielsweise durch beschleunigungssensorbasierende Reduktion der Bewegungsartefakte oder durch klinische Kalibrierung hinsichtlich der Messung der Sauerstoffsättigung, in Betracht gezogen werden.

Table of Content

1 Introduction

The aging of society and their growing cost pressure is one of the big future challenges of health care systems all over the world. Mobile devices and wearables, both equipped with various of sensors, could help resolving that problem in different scenarios. Those “smart”-devices can, for example, be used for self-monitoring purposes of individuals and therefore be used for both key elements of healthcare, prevention and rehabilitation.

This work is inspired by a previous project performed during the master studies in Digital Healthcare at the University of Applied Science, Sankt Pölten. The project focussed on the development of a low cost, real-time and multi-user system to monitor vital signs of a group of individuals simultaneously during physical exercises using the method of photoplethysmography (PPG). The monitoring of individual’s heart rate, heart rate variability and blood oxygen saturation (SpO_2) were key requirements of the developed system.

The developed device measures the pulse rate of individuals using red and infrared light instead of green light, which is used in most of commercially available pulse sensing mobile devices or wearables. This is considered as a main advantage of the prototype due to the theoretical possibility of sensing peripheral blood oxygen saturation as an additional vital sign based on reflected red and infrared light measurements. Especially in exercise therapy situations of patients with lung diseases, the oxygen saturation should be continuously monitored.

The aim of this work is to test and compare the performance of a new developed PPG device to current devices used for the detection of RR-intervals during a heartbeat and blood oxygen saturation values, respectively ECG and Pulse Oximeter. For this reason, a prototype of the above stated monitoring system has been developed, an experimental trial has been set up and the accuracy of the device has been analysed.

In this work, the performance of the developed prototype has been compared to reference devices. The heart rate, especially the intervals between each heart beat has been compared to an ECG sensor, which can be considered as the current “golden standard” for heart rate variability analysation. Furthermore, the blood oxygen saturation derived by the developed prototype has been compared to a commercially available pulse oximeter.

Referring to the previous described proceeding, the research question is formulated as follows:

- How reliable and accurate is the use of photoplethysmography (PPG) to record individual's peak-to-peak variations in the heart rhythm compared to electrocardiography?
- How reliable and accurate is the use of photoplethysmography (PPG) to record individual's blood oxygen saturation (SpO_2) compared to a commercially available device?

To answer the above stated research questions, five subjects in rest and moderate physical exercise phase have been tested. Each subject was equipped with a PPG, ECG and pulse oximeter devices. Raw PPG, ECG and blood oxygen saturation signals were recorded simultaneously. To determine the RR-intervals, the raw data were manipulated (interpolated, filtered and aligned) and peak-to-peak intervals were evaluated (detection, filtering and pairing of peaks). Individual's blood oxygen saturation was computed by evaluating the ratio between reflected red and infrared light.

The structure of this work is characterised by two main parts, a theoretical fundament as well as an experimental part. The first part includes chapter 2 and 3. Chapter 2 gives an overview on fundamental physiology of the heart and the circulatory system as well as an introduction in heart rate sensing techniques. The state of the art methods regarding to electrocardiography (ECG) and photoplethysmography (PPG) peak detection are described in chapter 3. The experimental part of this thesis includes chapters 4, 5, 6, 7 and 8. This part gives information about the process that lead to the experimental phase, the experiment itself, the analysis and interpretation of the results. The prototype development and the final prototype are described (chapter 4). The procedures for sensing and detection of the variables of interest, namely RR-Intervals and blood oxygen saturation values, are given in chapter 5. Chapter 6 deals with the description of the experimental setup and the algorithms developed to analyse the data and obtain the final results, which are described in chapter 7. Bland-Altman plots, which are the selected tool to verify if there is an agreement between the measurements performed by using different devices, is reported in chapter 8. Finally, the conclusions that can be drawn from this work are stated in chapter 9.

The following definitions are related to the main variable of interest object of this work.

RR interval in electrocardiography (ECG) is defined as the distance between two subsequent heart beats, more precisely the interval between R peaks in the QRS complex. A more detailed explanation of electrocardiography can be found in chapter “2.3.1 Electrocardiography (ECG)”. For better readability, peak-to-peak derived by both methods, ECG and PPG, are called “RR intervals”, even though peak-to-peak intervals in PPG signals are not corresponding to the QRS entity of ECG signals.

SpO_2 is defined as the percentage of the concentration in oxygenated blood cells (cHbO) compared to the sum of concentrations of reduced oxygenated blood cells (cHb) and oxygenated blood cells in arterial blood [7].

2 Physiological overview and heart rate sensing techniques

2.1 The heart

The heart is a muscular hollow organ which rhythmically pumps blood through the body. The right heart pumps oxygen-poor blood through the lungs while the left heart pumps oxygen-rich blood through the peripheral organs [1]. Figure 1 shows an illustration of the two pumps of the heart (left- and right heart) The contraction of the heart is controlled by a series of electrical impulses, originating from the sinoatrial node (SA node) and travels through the atrioventricular node (AV node) causing the polarization and depolarization of the heart's muscle fibres. These electrical impulses can be monitored and recorded as electrocardiogram (see "2.3.1 Electrocardiography (ECG)") [2].

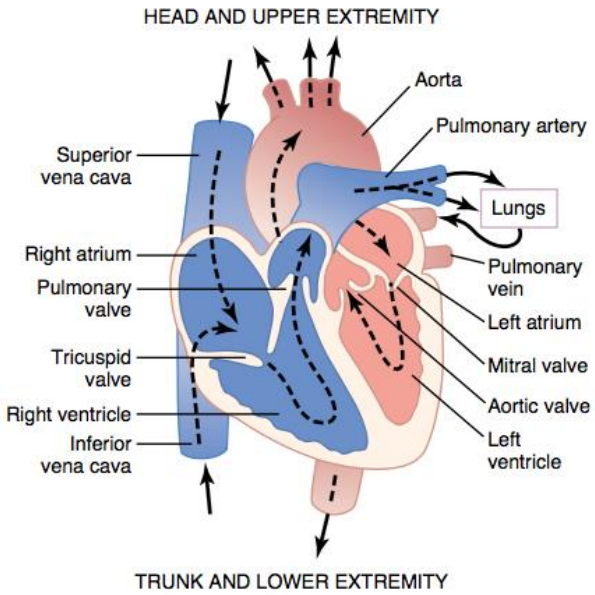

Figure 1: Structure and blood flow of the heart [1]

2.2 The circulatory system

The function of the circulatory system is to service the needs of the body tissues:

- to transport nutrients to the body tissues
- to transport waste products away
- to conduct hormones from one part of the body to another.

In general, the circulatory system maintains an appropriate environment in all the tissue fluids of the body for optimal survival and function of the cells. It is divided in systemic circulation and pulmonary circulation (see Figure 2). The systemic circulation supplies blood flow to all the tissues of the body except the lungs. The smaller pulmonary circulation is responsible for the oxygen enrichment of blood [1].

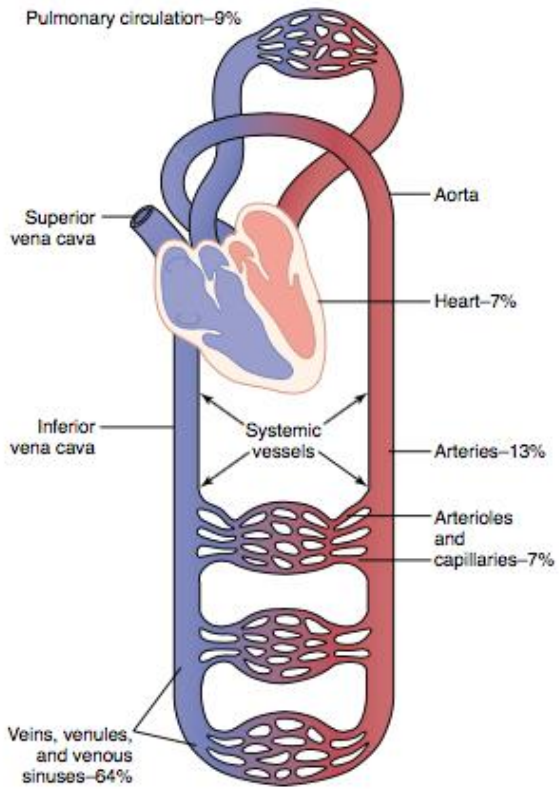

Figure 2: Distribution of the blood (pulmonary and systemic circulation) [1]

2.3 Heart rate sensing techniques

Various methods are used to measure and analyse the activity of the heart including Electrocardiography, Photoplethysmography, Oscillometry and Phonocaridography. The following sections describe the methods of Electrocardiography and Photoplethysmography in more detail and give an overview of other sensing techniques.

2.3.1 Electrocardiography (ECG)

While the cardiac impulse passes through the heart, electrical current spreads from the heart into the adjacent tissues surrounding it. A small amount of current spreads all the way to the surface of the body. The electrical potentials generated by the current can be recorded by placing electrodes on the skin on opposite sides of the heart. This recording is called electrocardiogram [1]. Therefore, electrocardiography is a method to record changes of the variations in the electrical potentials of the heart muscle. The common human heart beat is divided in three entities. Figure 3 shows the ECG of a usual heart beat including the entities [3].

The ***P wave*** is caused by the spread of depolarization through the atria, which is followed by the atria contraction causing a slight rise in the atria pressure curve immediately after the electrocardiographic P wave.

The ***QRS waves*** (also called the QRS complex) appears about 0.16 second after the onset of the P wave. It represents the electrical depolarization of the ventricles, which initiates its contraction and causes the ventricular pressure to begin rising (slightly before the onset of the ventricular systole).

The final ventricular ***P wave*** represents the stage of repolarization of the ventricles when the ventricular muscle fibbers begin to relax (slightly before the end of the ventricular contraction [1].

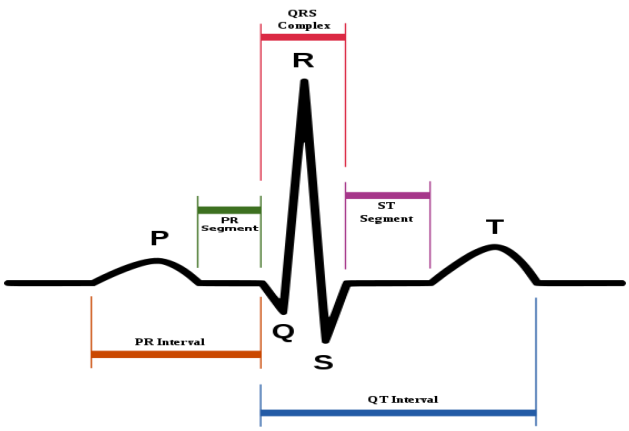

Figure 3: ECG of an usual heart beat [4]

2.3.2 Photoplethysmography (PPG)

Photoplethysmography is a simple and low-cost optical technique which can be used to determine blood volume changes in the microvascular bed of tissue. It is a widespread clinical application (e.g. pulse oximeters, vascular diagnostics and digital beat-to-beat blood pressure measurement systems), used non-invasively to make measurements on the skin surface operating at red or near infrared wavelength.

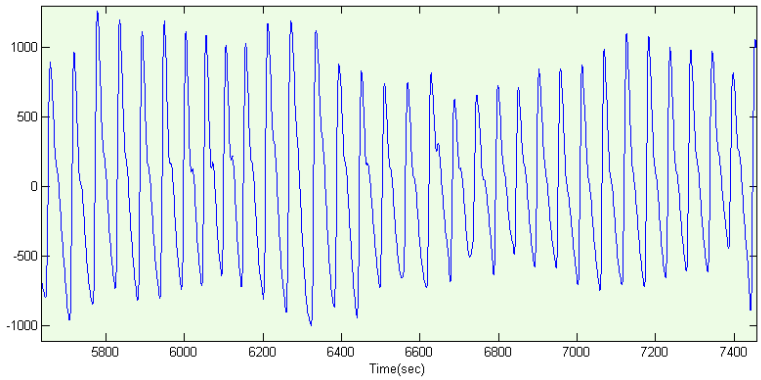

Figure 4: Photoplethysmogram form a pulse oximeter [5]

Figure 4 shows a representative photoplethysmogram including its most recognized waveform feature, the peripheral pulse which is synchronized to each heartbeat [6] [7].

Basic photoplethysmography requires two opto-electronic components, a light source and a photodetector. The light source is needed to illuminate the tissue (e.g. skin) and the photodetector to detect the small variations in light intensity (absorbance) accessioned with changes in perfusion in the catchment volume. Pulse oximetry mostly operates in red or/and infrared wavelength. Its most recognizable waveform feature is the peripheral pulse, which is synchronized to each heart beat [8]. The resulting pulsating photoplethysmography waveform is often called the “AC” component representing the heartbeat. This “AC” waveform is super imposed by a large quasi “DC” component that relates to the tissues and to the average blood volume. This “DC” component changes slowly depending on respiration, vasomotor activity and vasoconstrictor waves [6].

Beside the information about the cardiovascular system, PPG can also be used for measuring changes in the blood oxygen saturation. Pulse oximetry uses two monochromic light sources in different wavelength, one in the red and one infrared (IR) regions. These two light sources are set in relation to measure the saturation of peripheral oxygen (SpO_2). SpO_2 is defined as the percentage of the concentration of oxygenated blood cells compared to the sum of concentration in

reduced oxygenated blood cells (haemoglobin) and oxygenated blood cells in arterial blood [9].

Pulse oximeters can operate in two modes, the transmission and the reflectance mode. Devices operating in the transmission mode detect the transmitted light (through a medium, for example fingers or earlobe) using a photodetector opposite to the source LED, while the reflective pulse oximeters detect reflected light from tissue, bone or blood vessels [10].

2.3.3 Other techniques

2.3.3.1 Oscillometry

The technique of Oscillometry is mostly used for commercially available automated blood pressure monitors. They detect the amplitude of oscillations impinged on an arm cuff by brachial artery pulses. The underlying artery is occluded by inflating the cuff rapidly and then deflated gradually. The cuff pressure oscillations increase until they reach a peak and then they decrease. The cuff pressure at which the maximum oscillations occur relates to the mean arterial pressure [11].

2.3.3.2 Phonocardiography

A phonocardiogram (PCG) is the recording of the heart sounds resulting from its activity. Therefore, it allows important conclusions on the mechanical action of the heart. This technique is commonly used to detect heart lesions producing extra sounds like murmurs, clicks, snap, third and fourth heart sounds [12].

3 State of the Art

To cover the topic of heart rate monitoring including HRV (heart rate variability) analysis using photo plethysmography technology (PPG), an extensive literature research was conducted.

3.1 Electrocardiogram (ECG)

The most popular method of deriving the heart rate signal is to acquire the electrocardiogram (ECG) signal which can afterwards be analysed using appropriate software [13]. The ECG is considered as a gold standard in HRV analysis although frequent fluctuations in base line signal are present as well as frequent contamination of ECG signal due to electrode movement and electromyography (EMG) interference due to muscular activity [13].

3.2 Photoplethysmography (PPG)

The second popular method to acquire and analyse the HRV signals are heart rate belts and wrist monitors offered by Polar, Sagunto, Garmin etc. The reliability and accuracy of such methods in HRV analysis is well established in research literature [14]–[18]. In recent years, Photoplethysmography (PPG) has been established as a new method or possibility to measure and acquire HRV signals. PPG is performed by combining an infrared emitter and detector inside a probe placed on the forefinger. The infrared light is emitted through the blood vessels in the finger and reflected off the bone or tissue (Figure 5). A blood pressure signal is derived from the effect that the changing blood volume has on the reflected infrared light [13]. The utility of PPG as a reliable method for measurement of HRV is recent demonstrated in research literature [19], [20].

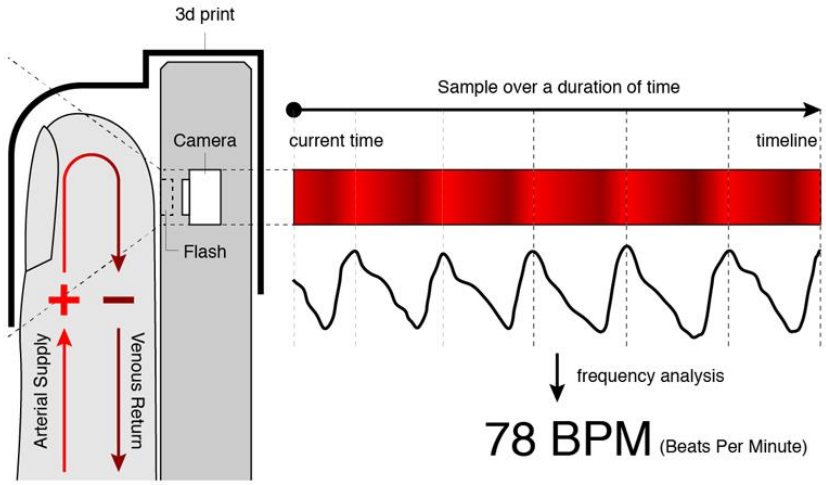

Figure 5: Photoplethysmography (PPG) Technology [21]

Shcherbina et al. [22] assessed the accuracy of seven commercially available wrist-worn devices, such as Apple Watch, Fitbit Surge, Microsoft Band etc., in estimating heart rate and energy expenditure (EE) to propose a wearable sensor evaluation framework. Their results show that most wrist-worn monitoring devices report heart rate with acceptable error range (5%) under controlled laboratory conditions of walking, running and cycling. Covariates such as darker skin tone, larger wrist circumference and higher BMI of the group of tested individuals were found to correlate positively with increased heart rate error rates across multiple devices. Device errors happened to be lower for running vs. walking but higher at higher levels of intensity within each modality [22].

Figure 6 shows the median error rate of wrist-worn devices across activities. An acceptable error range was defined as <5% (dark blue). Light blue, white and yellow shading indicates errors outside this range [22].

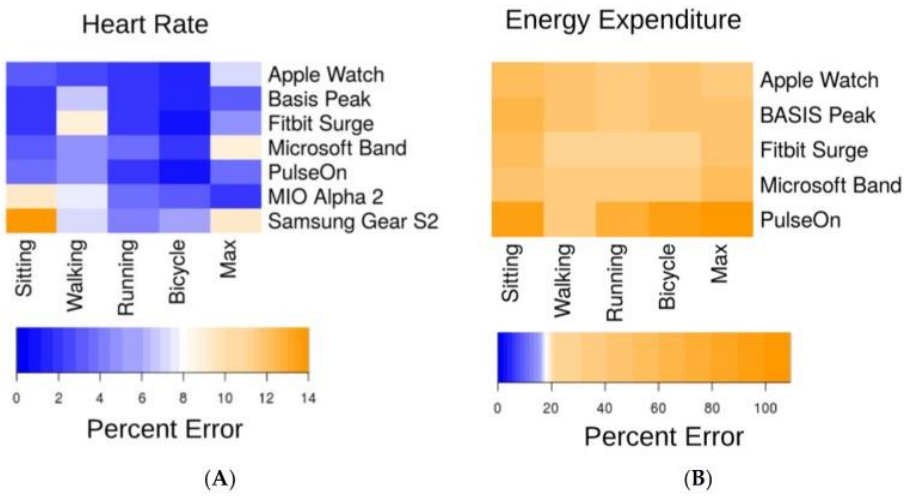

Figure 6: Median device error across activities

3.3 PPG vs. EEG

In the study of Bolanos et al. (2006), the agreement between PPG and ECG obtained HRV signals has been investigated [13]. The results from their study have demonstrated excellent agreement between those two methods and they have supported the idea of using PPGs instead of ECGs in HRV signal derivation and analysis in cardiac monitoring.

The same agreement was observed by Lu et al. (2008) [23]. They have simultaneously acquired PPG and ECG signals for ten healthy subjects. In conclusion, they have verified the feasibility of the PPG by comparing both time and frequency-domain parameters of the HRV, which all demonstrated high correlation between the two signals [23].

Furthermore, the significant positive agreement between heart rate belts and PPG in terms of HRV assessment was recently observed in the study of Vasconcellos et al. [15]. They have simultaneously conducted HRV recordings using ECG, PPG and Polar RS800cx watch. They demonstrated that HRV data obtained from Polar RS800cx and PPG appear to be as accurate and reproducible as data from ECG when evaluating the autonomic control of heart rate at rest [15].

Similar conclusion can be drawn from a study of Gonçalves et al., which compares ECG and PPG signals to evaluate signal loss and maternal heart rate (MHR) variability indices during the last two hours of labour. Their results show that signal loss was higher with ECG during the first segments of the first hour and higher with PPG in the last segment of the second hour. Signal loss increased in both signals with labour progression. MHR variability indices were significantly different when acquired with ECG and PPG signals. It shows low correlation coefficients and high disagreement for entropy and fast oscillation-based indices, and low disagreement for the mean MHR and slow oscillation-based indices. Nevertheless, the study considers PPG as an alternative for MHR monitoring during labour [24].

3.4 PPG peak detection

Elgendi et al. propose an algorithm that is more robust against effects of post-exercise measurement in non-stationarity during hot/humid conditions. The results show that the proposed method is able to detect systolic peaks correctly in non-stationary PPG signals before exercise. In case of non-stationary PPG signals produced after exercise, the algorithm did incur a few instances of failure. The cause of the failure is due to the extremely low amplitude systolic waves in heat-stressed PPG signals. They apply an event-related dual moving average for real-time application and processing of large databases [25].

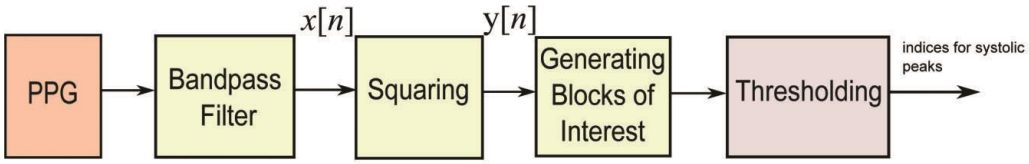

Figure 7: Flowchart for the proposed method/algorithm [25]

As Figure 7 shows, the signal is processed using a Bandpass Filter which removes the baseline wander and high frequencies. Squaring emphasises the large differences resulting from the systolic wave, while suppressing the small differences of the PPG signal. Blocks of interest are generated based on two moving averages, one to emphasise the systolic peak area while the second one is used as a threshold for the first moving average. Thresholding is used to eliminate blocks that are smaller than the expected width for the systolic beat duration, which are considered as noisy blocks.

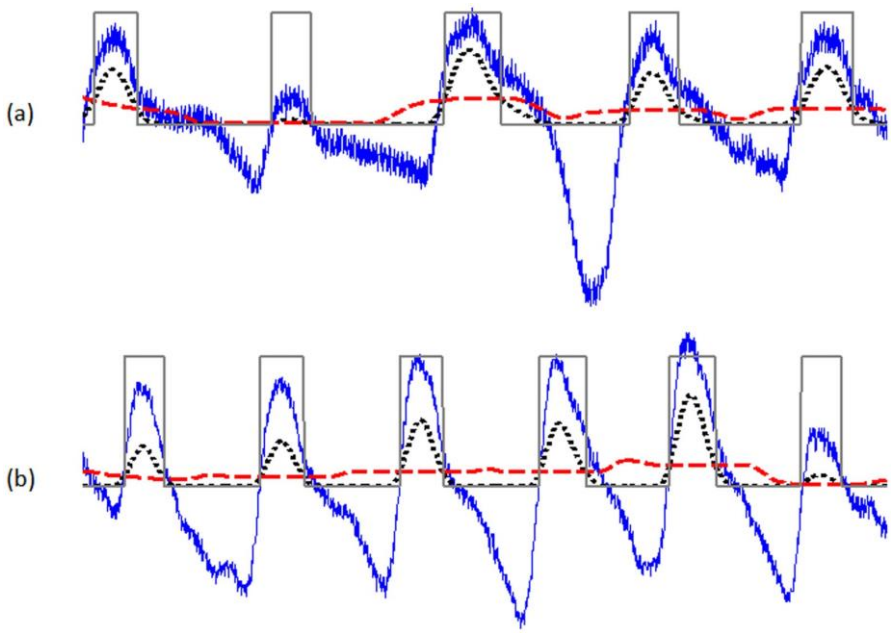

Figure 8: Blocks of interest based on two moving averages [25]

4 Hardware design and sensor technology

To achieve the ambition of a low cost real-time heart rate monitoring system, various sensors and microcontrollers were tested and evaluated. The following sections describe the progress of the development and the used hardware.

4.1 Sensor hardware

4.1.1 Early developments and prototypes

The first experiments and prototypes were developed using the 'e-Health Sensor Platform' offered by *cooking hacks*©, an online shop for electronics for makers (Do-it-yourself culture) and the education community [26]. Their *e-Health Sensor Platform* provides various biometric sensors for measuring vital signs like pulse and oxygen saturation, heart rate, muscle activity, glucose in blood, breathing, patient position, body temperature, sweating and blood pressure. The platform can be interfaced using an *Arduino* microcontroller or a *Raspberry Pi* microcomputer [27].

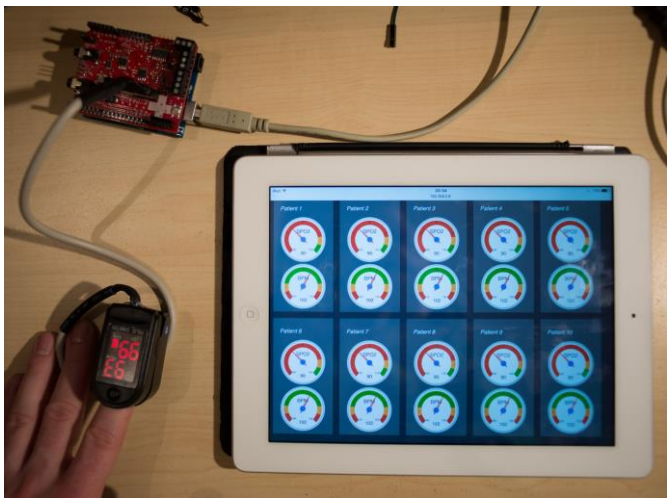

Figure 9: First experimental prototype

Figure 9 shows the very first experimental prototype using the *Blood and Oxygen in Blood Sensor* (lower left corner) attached to an Arduino microcontroller (upper left corner) which processes and monitors the heart rate and oxygen saturation signal. The first approach of hardware components could not be pursued due to the limitations of the used sensor. The sensor only provides calculated heart rate values in beats per minute which cannot be used for the calculation of the heart rate variability [28].

The next approach was the use of the commercially available Bluetooth finger-clip oximeter *Berry Pulse Oximeter BM1000C.* The sensor sends biometric data via Bluetooth and provides a BCI communication protocol for developers (see Figure 10) [29].

Byte	Bit	Description
1	0~3	Signal strength (0~8)
	4	1=no signal，0=OK
	5	1=probe unplugged, 0=OK
	6	1=pulse beep
	7	Sync bit=1
2	0~6	Pleth
	7	Sync bit=0
3	0~3	Bargraph
	4	Sensor off=1, 0=OK
	5	Pulse research=1, 0=OK
	6	Bit 6 of Byte 3 is bit 7 of the Pulse Rate
	7	Sync bit
4	0~6	Bits 0-6 of Byte 4 are bits 0-6 of the Pulse Rate
	7	Sync=0
5	0~6	SpO2 0-100%
	7	Sync=0

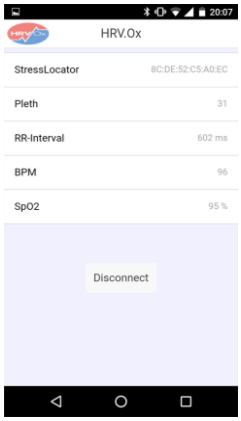

Figure 10: Berry Bluetooth Pulse Oximeter (left), technical specifications and BCI communication protocol (middle), developed mobile application (right)

A mobile Android application was developed in order to monitor and record the provided biometric data as the raw pulse signal, peak-to-peak interval in milliseconds and the peripheral oxygen saturation (SpO_2). A screenshot of the application is presented in Figure 10 (right). Despite the offered communication protocol and software development opportunities of this device, a significant signal loss was experienced during test-recordings. The device did not detect the same amount of heart beats compared to other devices, namely *Polar H7 chest strap* as well as the *ModernDevice sensor*. Therefore, the *Berry Bluetooth Pulse oximeter* resulted as inappropriate for accurate heart rate variability monitoring. During a concurrent recording of five minutes, the Berry Bluetooth Pulse Oximeter delivered 420 RR-interval values, while the self-implemented *ModernDevice sensor* delivered 580 values (see Figure 11).

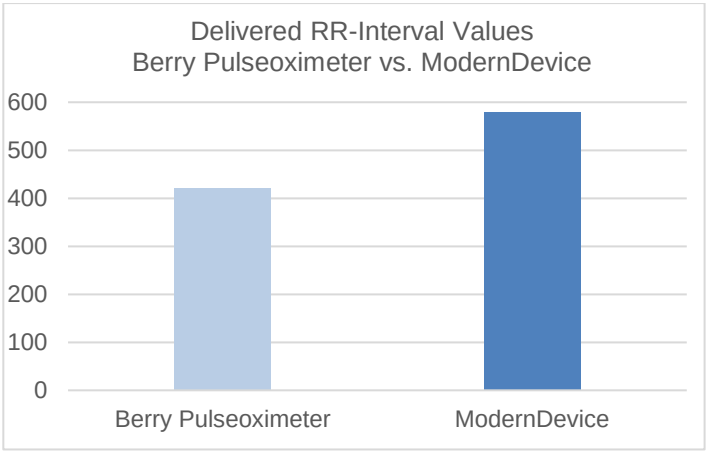

Figure 11: Comparison of delivered values for the RR-interval

4.1.2 Final Prototype

After the research and testing of various sensors, the most appropriate solution was combining the low-cost "*Pulse/SPO2*" sensor by *Modern Device*© and the Wifi-Microcontroller *Wemos D1 mini* which are described in the following subchapters.

4.1.2.1 Sensor

As mentioned above, the "*Pulse/SPO2*" sensor from *Modern Device*© (see Figure 12) was used for the final prototype. The sensor uses the Silicon Labs© SI1143 chip, which was originally designed for proximity sensing, but equipped with the necessary parts for pulse and oxygen saturation sensing. The sensor is outfitted with two infrared LEDs, one red LED and two photodiodes. LEDs in different wavelength are needed for sensing and calculating the oxygen saturation in blood (see chapter "5.1.2 Calculation of the blood oxygen saturation"). The chip provides digital control (I2C) over all resources [30].

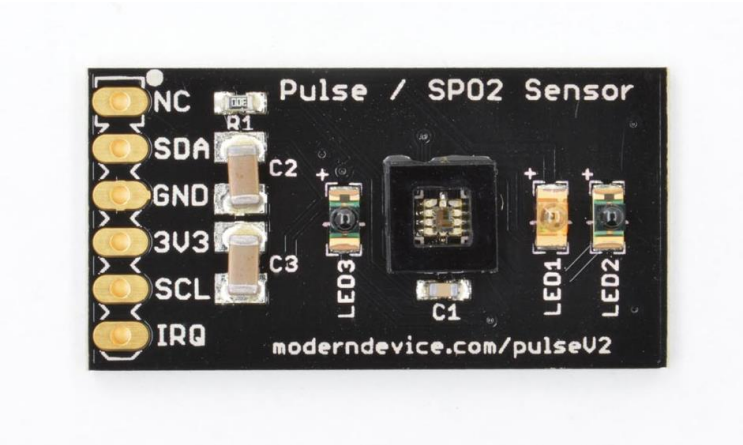

Figure 12: Modern Device's Pulse / SPO2 Sensor

4.1.2.2 Microcontroller

For signal processing and signal transmission a small Wi-Fi microcontroller board, based on the ESP-8266, was used [31]. The following subsections give a technical overview on the components of the developed device.

4.1.2.2.1 ESP-8266

The ESP-8266 is a microcontroller designed by the Chinese company *Espressif Systems*©. It advertises itself as a self-contained Wi-Fi networking solution offering itself as a bridge from existing microcontrollers to Wi-Fi. The original size of the chip makes impossible to use it for prototyping. Therefore various 3rd party, so called OEMs (Original Equipment Manufacturers), such as *Wemos*©*,* are taking those chips and building “breakout boards” for prototyping purposes [32]. Table 1 shows the technical specifications of the ESP-8266.

Table 1: ESP2-866 specifications [32]

Voltage	**3.3 V**
Current consumption	10uA – 170 mA
Flash memory attachable	16MB mag (512K normal)
Processor	Tensilica L106 32bit
RAM	32K + 80K
GPIOs	17 (multiplexed with other functions)
Analog to Digital	1 input with 1024 step resolution
802.11 support	b/g/n/d/e/i/k/r
Maximum concurrent TCP connections	5

4.1.2.3 Wemos D1 mini

Due to the ambition to keep the device as small and simple as possible the ESP8266 “breakout board” *Wemos*© *D1 mini* was used. The board measuring no more than 31x22 mm makes it one of the smallest WIFI-boards available on the market. Wemos© provides additional stackable sheets for further functionality such as battery shields, LED shields or micro SD card shields.

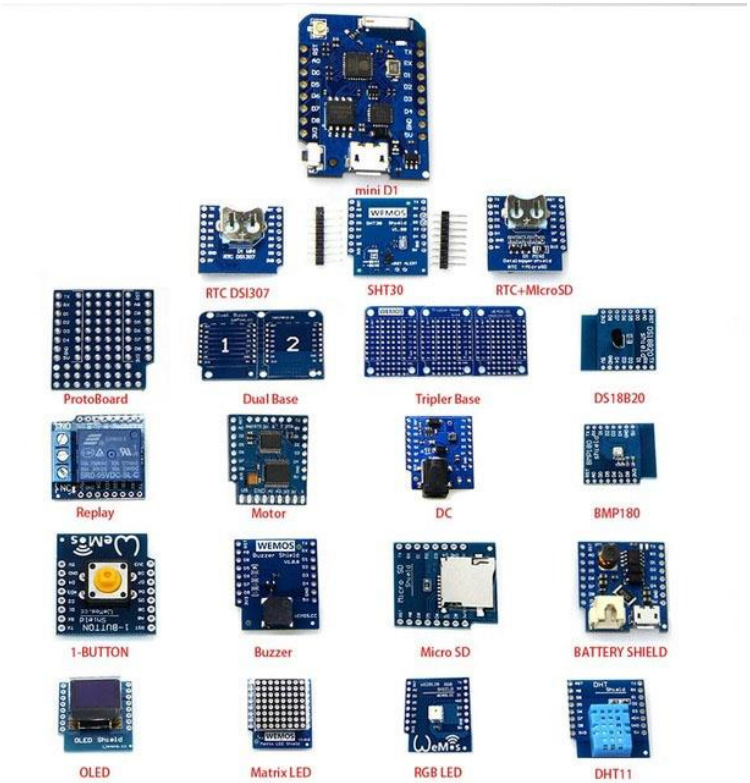

Figure 13: Wemos© D1 mini & available stackable shields [33]

4.1.2.4 Final setup

The final prototype includes the following hardware components:

- Wemos© D1 mini board (ESP-8266)
- Modern Device *Pulse/SpO2* (Silicon Labs© SI1143)
- Battery shield
- Lithium-ion polymer battery (3.7V / 700mAh)

Figure 14 shows the final prototype and its components. The Pulse/SPO2 sensor measures the light reflectance in the microvascular blood tissues. The Wemos© D1 mini is responsible for Wi-Fi-connection, I2C-communication with the Pulse/SPO2 sensor as well as signal processing. To provide a wireless device, a battery shield and a lithium-ion polymer battery supplies the device with power.

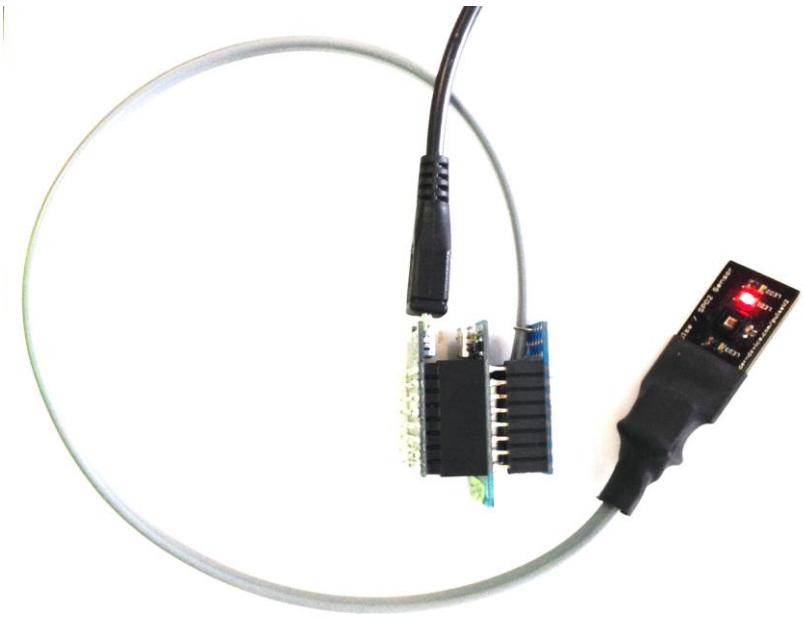

Figure 14: Final prototype and its components

5 Methodology

This chapter provides information on sensing, detection and evaluation of the variables of interest: RR-intervals and blood oxygen saturation.

5.1 Heart beat detection and the calculation of the blood oxygen saturation

As described in chapter “2.3.2 Photoplethysmography (PPG)” the developed device is capable of sensing the heart rate and the oxygen saturation. It operates in the reflective mode, and therefore detects the reflected light from tissue from the finger.

In the following sections, the proceeding for the detection of the heart beats as well as the calculation of the blood oxygen saturation values is explained.

5.1.1 Heart beat sensing & detection

5.1.1.1 Heart beat sensing

Only a very small amount of reflective light is responsible for sensing the pulsatile component of artery blood, which is used to calculate heart beats per minutes (bpm) as well as heart rate variability. Almost 90% of the applied light is reflected by skin and tissue [34], [10].

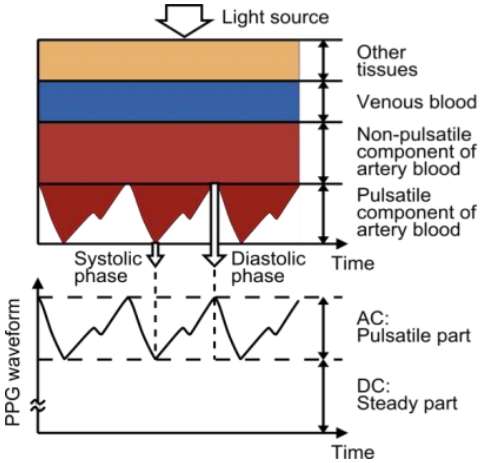

Figure 15: Variation in light attenuation by tissues of blood [10]

Figure 15 shows an example of a photoplethysmographic waveform divided in layers depending on the tissues of blood. Most changes in blood flow occur

primarily in the arteries and arterioles and not in the veins. For instance, arteries contain more blood volume during the systolic phase of the cardiac cycle than during the diastolic phase which can be observed in the PPG waveform [10].

5.1.1.2 Heart beat detection

As mentioned above, arteries widen and contract with each heart beat. During the systole, the phase in which the ventricle of the heart contract and blood pressure rises, the relatively thicker arteries increase the absorption of light. During diastole, when the ventricle of the heart relaxes and the blood pressure falls, the relatively thinner arteries decrease the absorption of light. To perform heart rate variability analysis and to calculate the beat per minute, the valleys between two heart beats have to be measured and calculated. For an accurate detection of peaks and valleys, the following steps should be applied [34]:

- **Low and High Pass Filtering**

  Low and high pass filtering helps to remove noise resulting from the environment (e.g. ambient light or electromagnetic interferences).

- **Separation of the AC part**

  Due to possible motion artefact, the baseline shifts during the measurement making more difficult to detect peaks and valleys. Therefore, the baseline should be computed e.g. by averaging the signal over time. The AC part can be isolated by subtracting the computed baseline of the total signal.

- **Moving average filtering**

  To smooth the resulting waveform from the steps above, a simple moving average filter can be applied.

5.1.2 Calculation of the blood oxygen saturation

To calculate the oxygen saturation of the blood (SpO_2), instead of summing up the signals of both wavelength, they are set in relation. SpO_2 is defined as the percentage of the concentration in oxygenated blood cells (c_{HbO}) compared to the sum of concentrations of reduced oxygenated blood cells (c_{Hb}) and oxygenated blood cells in arterial blood [9]:

$$SpO_2 = \frac{c_{HbO}}{c_{HbO} + c_{Hb}}$$

Equation 1

It is possible to use reflected light to calculate SpO_2 thanks to the haemoglobin within red blood cells. Those cells are essential for oxygen transport by blood,

since they carry about 97% of the blood's oxygen. In the human blood, different species of haemoglobin are present which are distinguished as functional and dysfunctional haemoglobin. Functional haemoglobins are able to bind oxygen reversibly. A fully saturated haemoglobin is revered to as oxyhaemoglobin (HbO) while all other not fully saturated functional haemoglobins are called reduced haemoglobin (Hb) [35]. This oxygenated haemoglobin can be detected over the reflection of red light. By measuring the ratio of absorbance of light at two wavelengths $A_{\lambda 1}$ and $A_{\lambda 2}$ where oxyhaemoglobin and reduced haemoglobin have different absorption coefficients, the ratio of oxygenated haemoglobin to total haemoglobin can be determined [36], [37]:

$$R = \frac{A_{\lambda 1}}{A_{\lambda 2}}$$

Equation 2

The wavelength of red and infrared light meet with the above stated requirements. Figure 16 shows the different absorption spectra for oxyhaemoglobin and deoxyhaemoglobin at the two wavelengths of red and infrared light.

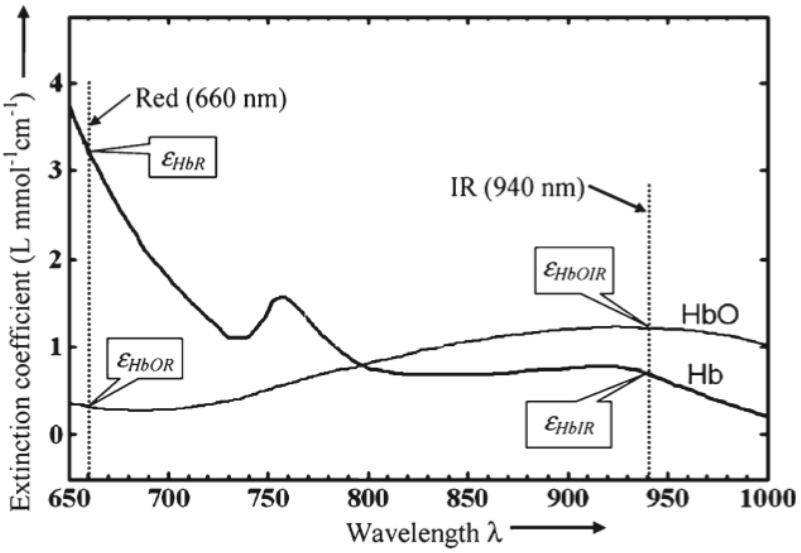

Figure 16: Absorption spectra of Hb and HbO [9]

The ratio between the concentrations of the deoxygenated blood and oxygenated blood is proportional to the ratio of red light absorption and the infrared light absorption. To receive the absorbance information $A_{\lambda 1}$ and $A_{\lambda 2}$ the Beer-Lambert law can be used, which states that the absorbance A results from the relationship between the light of intensity I_0 and the emitted light I_1 after passing I_0 through an absorbing medium:

$$A = \ln\left(\frac{I_0}{I_1}\right) = \varepsilon c d$$

Equation 3

ε represents the extinction coefficient, which relates to the light absorption of the medium while d is the distance travelled by the light (cm) and c is the concentration of the absorbing medium (mol/L). By using the ratio of light measured by the photoreceptor at the peak ($I_{\lambda high}$) and through ($I_{\lambda low}$) of the heartbeat cycle, it is possible to obtain independent information of the absolute light intensity I_0 of the light emitting diode and independent of tissue that do not contain arterial blood.

The total absorbance of a mixture of elements with varying absorbencies can be determined using the Beer-Lambert law as the sum of individual absorbencies:

$$A_\lambda = \varepsilon_{\lambda Hb} c_{Hb} d + \varepsilon_{\lambda HbO} c_{HbO} d$$

Equation 4

By combining equations Equation 3 and Equation 4 the ratio between red and infrared absorbencies can be written as:

$$A = \frac{A_R}{A_{IR}} = \frac{\ln\left(\frac{I_{Rhigh}}{I_{Rlow}}\right)}{\ln\left(\frac{I_{IRhigh}}{I_{IRlow}}\right)} = \frac{\varepsilon_{RHb} c_{Hb} + \varepsilon_{RHbO} c_{HbO} d}{\varepsilon_{IRHb} c_{Hb} + \varepsilon_{IRHbO} c_{HbO} d}$$

Equation 5

Substitute c_{Hb} and c_{HbO} by the function of arterial oxygen saturation by using Equation 6 to derive R as a function of SpO_2:

$$R = \frac{\varepsilon_{RHb} + (\varepsilon_{RHbO} - \varepsilon_{RHb}) SpO_2}{\varepsilon_{IRHb} + (\varepsilon_{IRHbO} - \varepsilon_{IRHb}) SpO_2}$$

Equation 6

The rearranged equation gives as result the theoretical saturation from the ratio of the measured, normalised absorptions in red and infrared light:

$$SpO_2 = \frac{\varepsilon_{RHb} - \varepsilon_{RHbO} R}{\varepsilon_{RHb} - \varepsilon_{RHbO} + (\varepsilon_{IRHbO} - \varepsilon_{IRHb}) R}$$

Equation 7

The values needed for the evaluation of the ratio depend on the absorption coefficient of deoxygenated and oxygenated haemoglobin (λ) and on the percentage of the haemoglobin which is oxygenated (R). The value of R is calculated from the four parameters derived from the sensor and the absorbencies

values are known and given as a function shown in Figure 16. The values of the two wavelengths most commonly used in pulse oximetry are:

Table 2: Common wavelengths used in pulse oximetry and relative coefficients

Wavelengths	ε_{Hb}	ε_{RHbO}
660 nm	0.81	0.08
940 nm	0.18	0.29

As mentioned above, the Beer-Lambert law is based on an approximation concept which states that the sum of transmitted and absorbed light is equal to the incident light. The incident light passing through human tissue is not only split into absorbed and transmitted light, e.g. some parts of the light are reflected, others are scattered. The Beer-Lambert law does not take these physical concepts into account and therefore the theoretical oxygen saturation differs from the empirical one as can be seen in Figure 17.

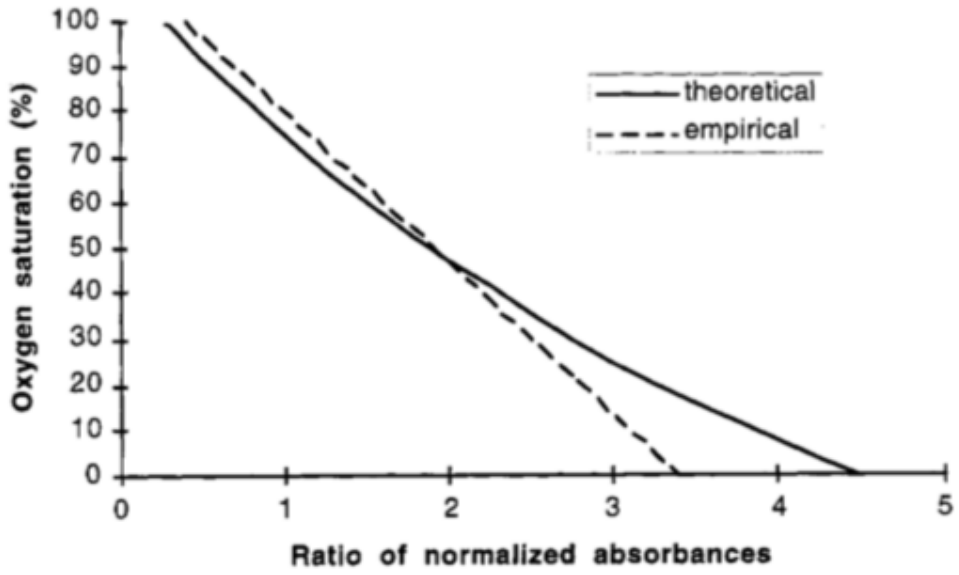

Figure 17: Calibration curves for pulse oximeters [2]

6 Implementation, Testing

6.1 Experimental setup

Five different individuals (two female and three male participants) have been tested in “rest” and “stress” phases. During the “rest” phase, the subject is sitting, while in the “stress” phase, the subject rides a stationary bicycle (Crane exercise bike; Model: RB#35301). On the above-mentioned device, it is possible to set the intensity of the pedalling within a range that goes from 1 (minimum value, lightest intensity) to 8 (heaviest intensity). The selected value for the test is equal to 4.

Table 3 gives an overview of the group of tested individuals considering mean age, height and body mass as well as the corresponding standard deviation.

Table 3: Demographic information of subject

	Age [y]	**Height [cm]**	**Body Mass [kg]**
Mean value	29	175	83
(±SD)	(±SD 18.67)	(±SD 9.975)	(±SD 11.415)

Each subject is equipped with:

- Developed PPG prototype on the right index finger;
- ECG device, as described more in details in the paragraph “6.1.1.2 ECG”;
- Pulse oximeter device on the right middle finger.

Data acquired form PPG and ECG devices have been analysed and compared to evaluate the heart rate of each subject in each test condition. Data acquired using PPG and Pulse Oximeter devices have been analysed to determine the blood oxygen saturation value and then compared.

The devices have been started simultaneously and data have been recorded for 6 minutes. The measurements were started manually while each signal delivered an accurate time stamp in milliseconds (synchronised before each measurement) to synchronise the signals manually after the recordings using that time information. The initial and final 30 seconds have been cut to eliminate any fluctuations of the results due to possible non-stationary behaviour of the measuring devices, the central 5 minutes of the recordings have been analysed.

6.1.1 Process of Data Acquisition

6.1.1.1 PPG

The PPG signal of the developed prototype was acquired using serial communication. The real-time data was logged and stored as a text file using a sampling frequency of 300Hz. Table 4 shows four exemplary lines of the recorded PPG signals. Column 1 (Time) and 2 (Time [ms]) are essential for synchronising the recording with other measurement methods.

Column 1 represents the Time in Hours, Minutes and Seconds while Column 2 represents the internal milliseconds of the ESP2866 microcontroller. Columns 3 to 5 (Red, IR1, IR2 and total) show the actual measurement in different wavelengths representing the three LEDs (Red, Infrared1 and Infrared2) of the photodiode while Column 6 is the sum of all wavelength measurements.

Table 4: Exemplary recorded PPG signal in text file

Time [hh:mm:ss]	**Time [ms]**	**Red [660nm]**	**IR1 [940nm]**	**IR2 [940nm]**	**Total**
17:46:56	3775368	29189	9501	16933	55623
17:46:56	3775372	29191	9501	16933	55625
17:46:56	3775375	29197	9504	16942	55643
17:46:56	3775378	29202	9511	16936	55649
Sampling frequency [Hz]			300		

6.1.1.2 ECG

The ECG signal was acquired using Plux®'s *BITalino Revolution Plugged Kit*, a low-cost vital sign reading platform. The ECG signal was measured using three gelled, self-adhesive, disposable Ag/AgCl chest electrodes [38].

The following electrodes placement was used:

- Positive electrode: under right clavicular (under the right collar bone);
- Negative electrode: under left musculus pectoralis major (under left pectoral muscle);
- Reference electrode: under left clavicular (under the left collar bone).

The signal was sent using a sampling frequency of 1000Hz using Plux®'s free to use software *OpenSignals (r)evolution*. The signal was sent via Bluetooth in real-time to the application and stored in an additional text-file. Table 5 shows the recorded ECG signal. Column 1 and 2 indicate the time information while column 3 refers to the measured ECG signal.

Table 5: Exemplary recoded ECG signal in text file

Time	Time [ms]	ECG signal [mV]
13:05:06.001	1	577
13:05:06.002	2	578
13:05:06.003	3	578
13:05:06.004	4	579
Sampling frequency [Hz]	1000	

6.1.1.3 SpO_2

The oxygen saturation of the peripheral blood was acquired using a *Berry® Pulse Oximeter BM1000C,* the same as used in early prototyping stages (see "4.1.1 Early developments and prototypes"). The device delivers every second SpO_2 values as well as the calculated participant's heart rate in beats per minute (see Table 6: Exemplary recoded SpO2 signal in text file).

Table 6: Exemplary recoded SpO_2 signal in text file

Time [dd:mm:yyyy] [hh:mm:ss]	SpO2 [%]	BPM (beats per minute)
15/09/2017 13:05:06	97	65
15/09/2017 13:05:07	97	66
15/09/2017 13:05:08	97	66
15/09/2017 13:05:09	98	66
Sampling frequency [Hz]	1	

6.2 MathWorks® MATLAB® Script

The analysis of the raw data has been performed using two scripts developed in a MATLAB® environment. The first script allows the detection of the heart beat

through the signals acquired using the ECG and the PPG devices. With the second script, it is possible to manipulate data obtained using the PPG sensor to evaluate blood oxygen saturation values and, therefore, to compare these results to the one obtained with the Pulse Oximeter device.

The procedure for RR-intervals and for blood oxygen saturation evaluation is described in the following paragraphs. The charts showed are examples taken from the results of a singular subject in the “rest phase”, but they can be generalised also to the other results.

6.2.1 Algorithm for RR intervals evaluation

The algorithm for the RR intervals evaluation is summarised in the figure below.

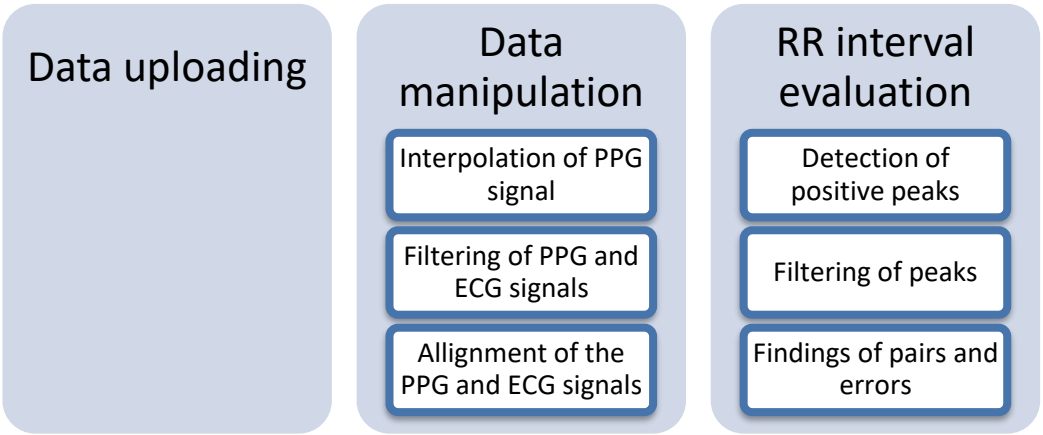

Figure 18: Algorithm for RR interval detection

The 5 minutes recorded data are uploaded in the form of a matrix.

The following figure shows how the raw data, without any manipulation, look like.

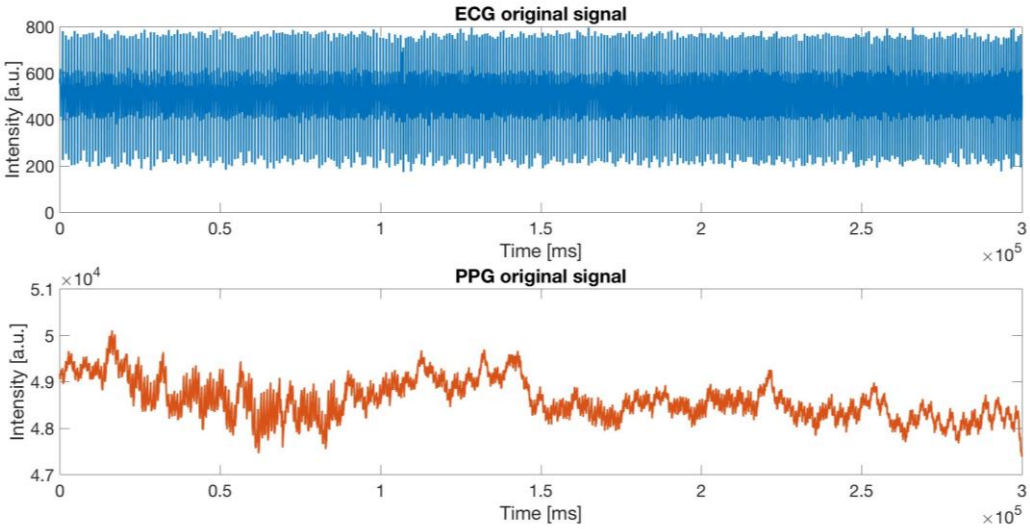

Figure 19: ECG and PPG signals, raw data

The ECG and PPG devices are characterised by two different sampling rates, namely the ECG has a higher sampling rate than the PPG signal. The ECG and PPG vectors have two different lengths and it is necessary to interpolate the PPG signal, in order to obtain a vector with the same length as the ECG one's.

Listing 1: *Increasing PPG signal's sampling rate*

```
Xq = (1:1:ECGlength);
PPGinterp = interp1(PPGtime,PPGtotal,Xq,'pchip');
```

Matlab®'s "interpl" function increases the original sampling rate of a sequence to a higher rate. The function returns a vector of interpolated values PPGinterp corresponding to the query points in Xq (time vector of the ECG recording). The values of PPGinterp are determined by shape-preserving piecewise cubic interpolation of PPGtime (time vector of the PPG recoding) and PPGtotal (sum of the derived PPG recording – red and two times infrared red) [39], [40].

After the interpolation of the PPG signal, the two vectors have the same length and the result is showed in Figure 20.

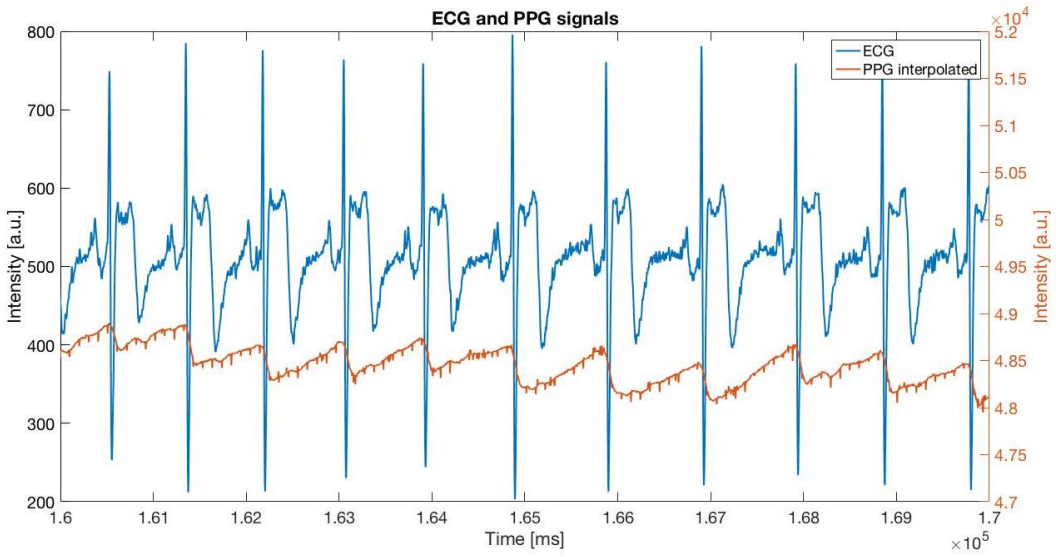

Figure 20: ECG and PPG (interpolated) signals

The two signals have to be filtered in order to make the process of peak detection easier and more effective. The MATLAB® function butter returns the transfer function coefficients bPPG and aPPG of a 2nd-order low pass digital Butterworth filter with a lower cut-off frequency of 0.8 Hz and a higher cut-off frequency of 8 Hz [41]. Filtfilt performs a zero-phase digital filtering by processing the input PPG data PPGinterp, in both the forward and reverse directions [42]. This latter reduces the noise in the signal and preserves the occurring of the peaks at the same time as it occurs in the original. With conventional filtering the noise would be reduced but there would be also a delay in the occurrence of the peaks. The filter reduces the baseline wander and high frequencies that do not contribute to the systolic peak [43]. Listing 2 shows the part of the MATLAB® code for filtering the PPG as well as the ECG signal.

Listing 2: *Filtering of ECG and PPG signals*

```
[bPPG,aPPG]=butter(2,[0.8, 8]/500);
filteredPPG = filtfilt(bPPG,aPPG,PPGinterp);

[bECG,aECG]=butter(2,[4, 50]/500);
filteredECG = filtfilt(bECG,aECG,ECG(:,1));
```

Both ECG and PPG signals are filtered and normalised. Figure 21 below shows the result of these operations.

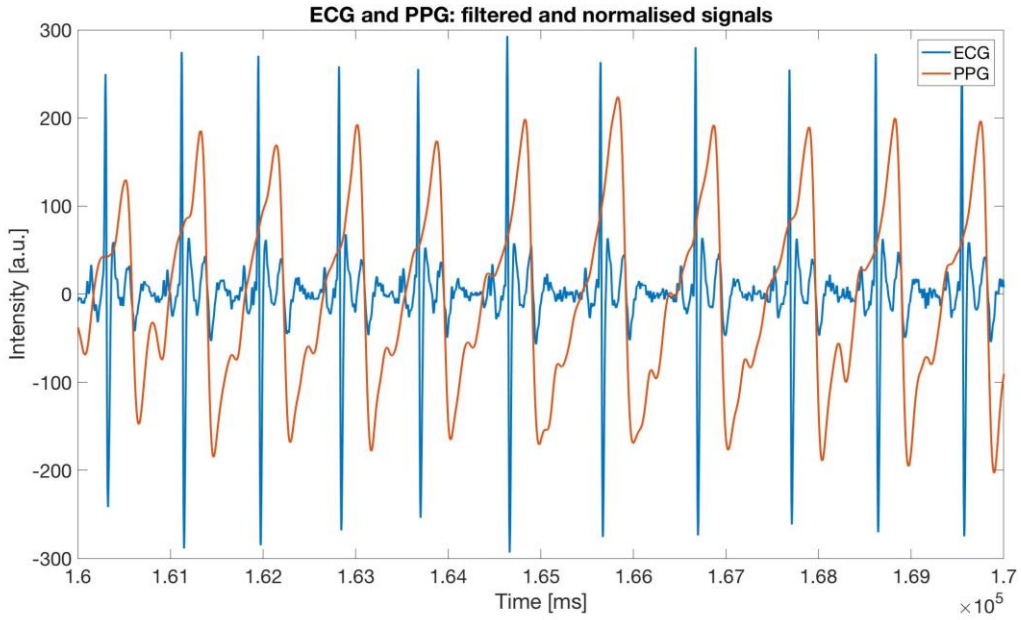

Figure 21: ECG and PPG signals, filtered and normalised

The alignment of the two signals is performed using the cross-correlation “xcross” function. The cross-correlation of two discrete time-sequences allows to find the similarities in the signals and to measure the lag time between them [44].

Listing 3 describes the alignment of the ECG and the PPG signals. The cross-correlation of the two signals is maximum at a lag equal to the delay ([~,I] = max(abs(acor));). Then the lag-difference is expressed as number of samples lagDiff as well as in seconds timeDiff. Finally the signal (s1al) and time (t1al) vectors can be aligned [44].

Listing 3: *Alignment of the ECG and PPG signals*

```
s2 = filteredPPG;
s1 = filteredECG;
Fs = 1000;

t1 = (0:length(s1)-1)/Fs;
t2 = (0:length(s2)-1)/Fs;

[acor,lag] = xcorr(s2,s1);

[~,I] = max(abs(acor));
lagDiff = lag(I);

timeDiff = lagDiff/Fs;

s1al = s1(-lagDiff+1:end);
```

```
t1al = (0:length(s1al)-1)/Fs;
```

Figure 22 shows the result of the aligning process. It is possible to see the ECG signal (blue line) aligned to the PPG (red line) and the ECG not aligned signal (yellow line).

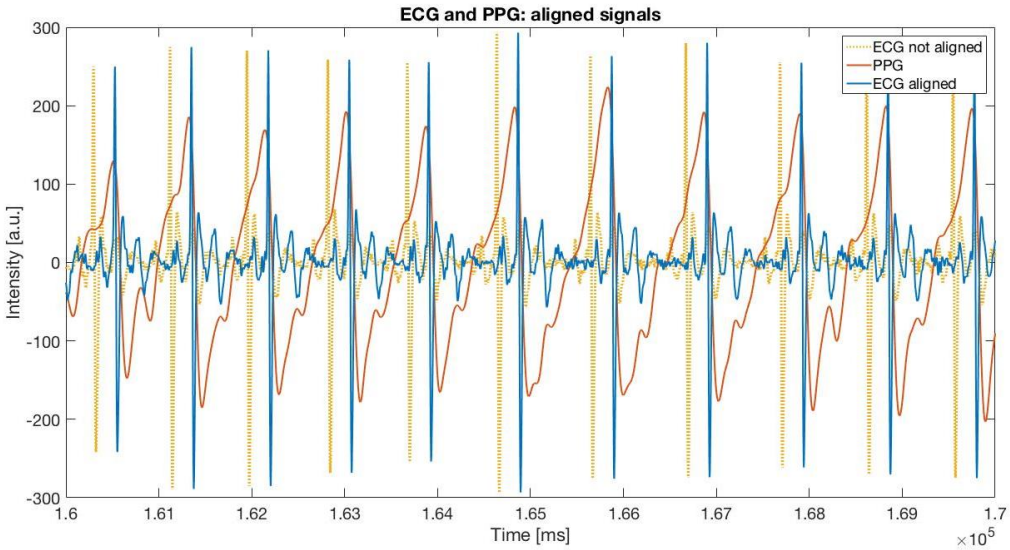

Figure 22: ECG and PPG aligned signals

At this stage, peak detection is performed: positive peaks are evaluated for the two signals.

Listing 4: *Positive peaks evaluation*

```
findpeaks(s1al,'MinPeakProminence',150, 'MinPeakDistance',300);
[pksECG,locsECG]=findpeaks(s1al,'MinPeakProminence',150,
'MinPeakDistance',300);
hold on
findpeaks(s2,'MinPeakProminence',100,'MinPeakDistance',300);
[pksPPG,locsPPG]=findpeaks(s2,'MinPeakProminence',100,'MinPeakDistance',30
0);
```

The “findpeaks” function is used to detect the peaks in the signals and two additional input parameters are selected: “MeanPeakPromincence” and “MeanPeakDistance”. The first allows to set the mean peak prominence, namely the amplitude, of each peak, in such a way that small peaks not relevant to the RR-intervals evaluation are detected. The “MeanPeakDistance” is used to set the mean distance between two peaks and it is also used to reduce the possibility of mistaken peaks.

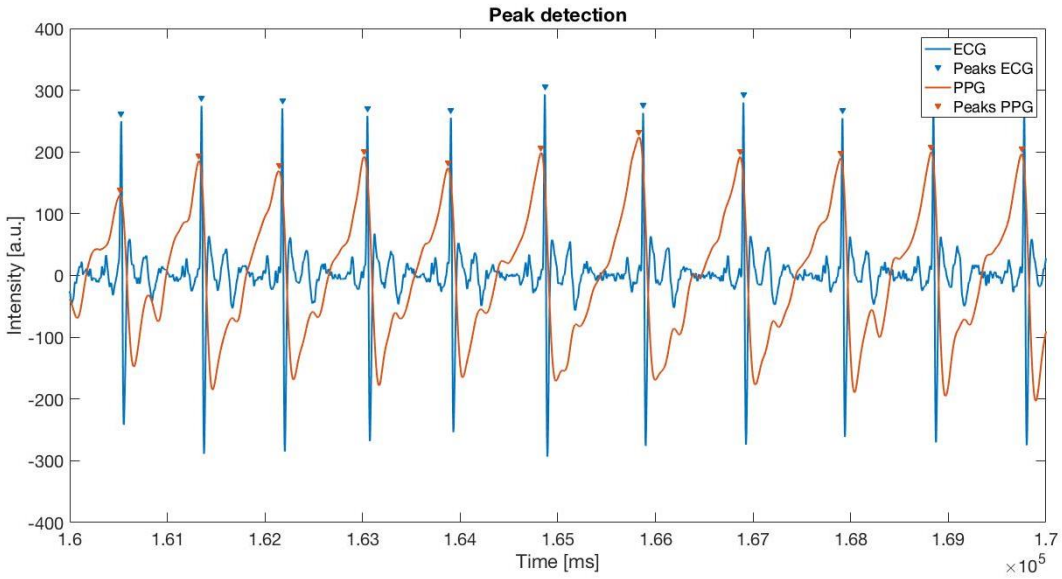

Figure 23: ECG and PPG peak detection

After the peaks evaluation, it is necessary to find the “pairs” between them. The ECG is considered as a “master” signal and the average distance between the peaks is evaluated. Then, each ECG peak is coupled to a PPG peak if the distance between them is less than to 30% of the average distance. When this condition is not verified, the peak in the PPG signal is considered as an “error” and, therefore, it is not taken into account for the RR-interval evaluation. The same considerations are valid for the ECG peaks detection.

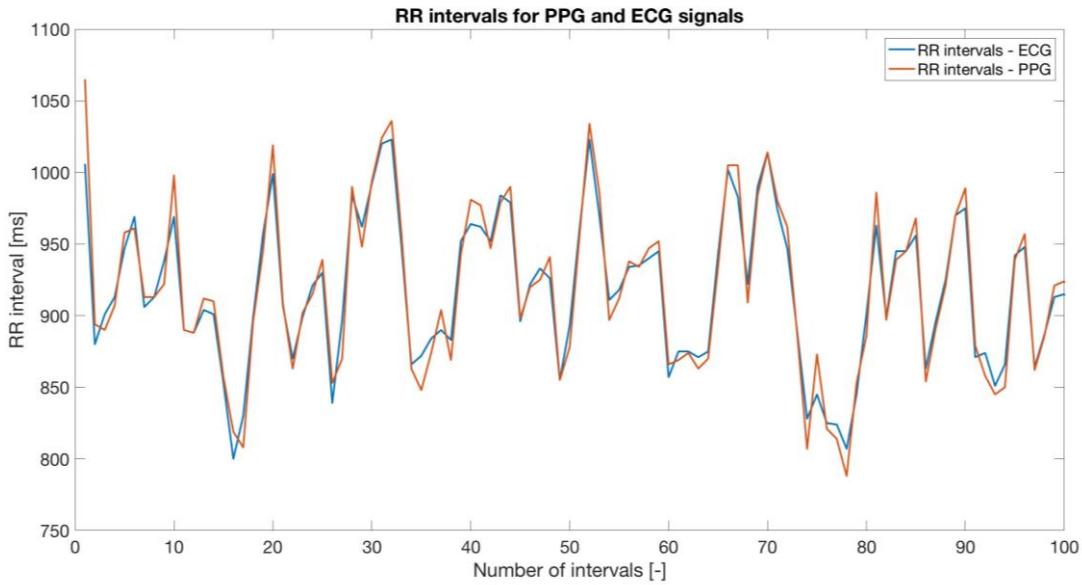

Figure 24: RR-intervals detection for ECG and PPG signals

Figure 24 shows the RR-intervals evaluated for the PPG and ECG signal. It is possible to notice that they are in good agreement.

6.2.2 Algorithm for blood oxygen saturation evaluation

The summary of the procedures followed to evaluate the blood oxygen saturation values are described in the figure below.

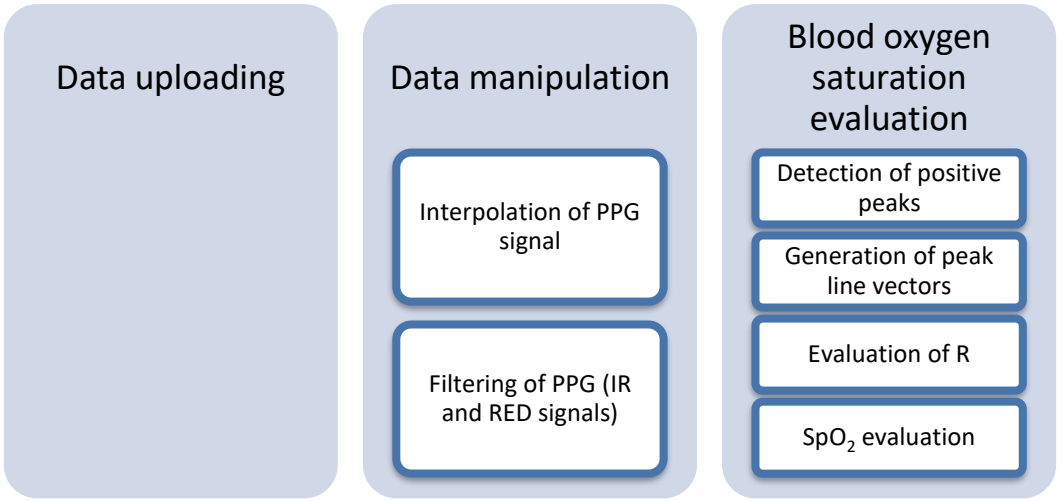

Figure 25: Algorithm for blood oxygen saturation evaluation

Data concerning the 5 minutes' recordings obtained using simultaneously PPG and Pulse Oximeter devices have been uploaded in the form of a matrix.

The PPG device gives as outputs values related to the red, infrared and total reflected light. The theoretical background regarding the blood oxygen saturation evaluation is given in chapter "5.1.2 Calculation of the blood oxygen saturation". The following evaluations have been performed taking into account Equation 5 and Equation 7.

The Pulse Oximeter device gives as output a blood oxygen saturation value every second. The sampling rate of the PPG device is equal to 300 Hz; therefore, an interpolation of the PPG signal is necessary to have corresponding values between the two signals.

After the interpolation, the two signals are filtered, as follows.

Listing 5: *Interpolation and filtering of the red and infrared PPG signals*

```
Xq = (1:1:300001);
REDinterp = interp1(time,red,Xq,'pchip');
IR2interp = interp1(time,ir2,Xq,'pchip');

[bPPG,aPPG]=butter(2,[0.8, 8]/500);
```

```
REDfiltered = filtfilt(bPPG,aPPG,REDinterp);
IR2filtered = filtfilt(bPPG,aPPG,IR2interp);
```

The result of these manipulations is shown in Figure 26.

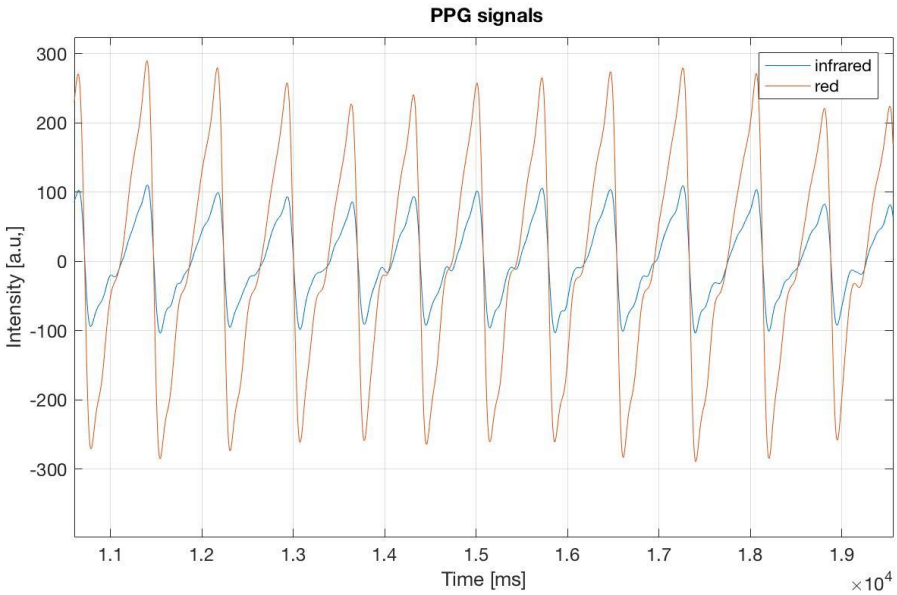

Figure 26: Red and infrared signals, interpolated, filtered

The calculation of the blood oxygen saturation values requires the evaluation of positive peaks of the curves shown in the figure above (see Figure 26).

The “findpeaks” function is used to evaluate the intensity of the peaks and their locations on the x axis. The above-mentioned function requires “MinPeakProminence” and “MinPeakDistance” values. Listing 6 shows the developed code for the peak detection of the red and infrared light.

Listing 6: *Evaluation of the positive peaks of the red and infrared signals*

```
minpeakdistance = 450;
minpeakprominence = 13;
minpeakprominenceIR = 20;

[pksIR2,locsIR2]=findpeaks(filteredIR2,'MinPeakProminence',
    minpeakprominence,'MinPeakDistance',minpeakdistance);
hold
[pksRED,locsRED]=findpeaks(filteredRED,'MinPeakProminence',
    minpeakprominence,'MinPeakDistance',minpeakdistance);
```

After the evaluation of peaks in both wavelength (red and infrared), a continuous vector representing the peaks was computed. Figure 27 shows the detected peaks (“peaks IR” and “peaks red”) as well as the computed, continuous peak vector

(“peak line IR” and “peak line red”) which is essential for calculating the ratio between both signals.

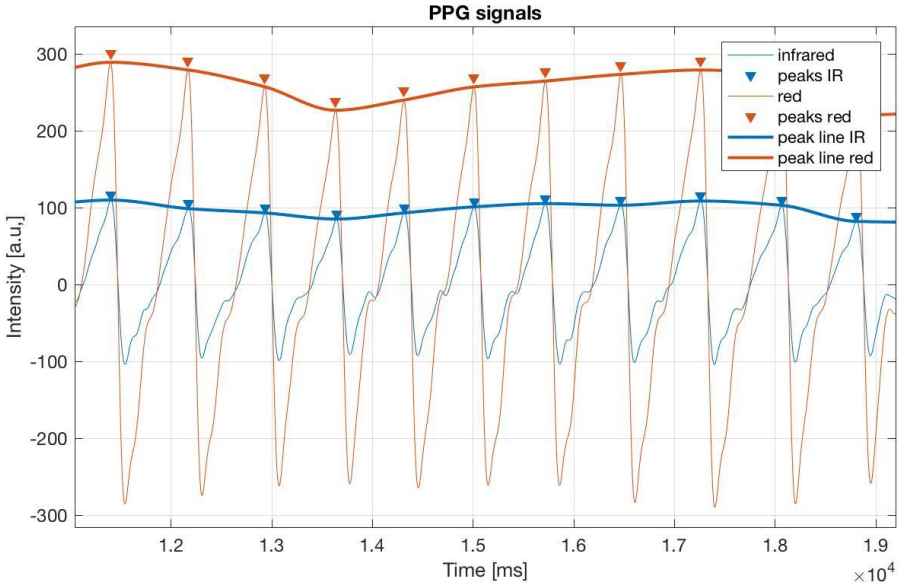

Figure 27: Detection of positive peaks and computed peak lines

A mean value for each second (1000 samples) of the computed peak signal was used in order to make it fit to the reference value derived from Berry©’s Pulse Oximeter sampling rate. The ratio of the signals was calculated using Equation 5 described in chapter “5.1.2 Calculation of the blood oxygen saturation”.

Listing 7: Computing mean vector, ratio, and filtered ratio

```
n = 1000;
meanIR = arrayfun(@(i) mean(pksREDinterp(
                                i:i+n-1)),1:n:length(pksREDinterp)-n+1);

meanRED = arrayfun(@(i) mean(pksREDinterp(
                                i:i+n-1)),1:n:length(pksREDinterp)-n+1);

ratio = log(meanIR).*(log(meanRED).^-1);

ratioFiltered = smooth(ratio, 0.3, ‘rloess’);
```

The derived ratio was filtered by MATLAB©’s smooth function using rloess as method, which assigns lower weight to outliers in the regression. This procedure helps to remove occurred motion artefacts. Figure 27 shows the computed ratio (blue line), the filtered ratio (red line) and motion artefacts (red circles) in the original raw signal.

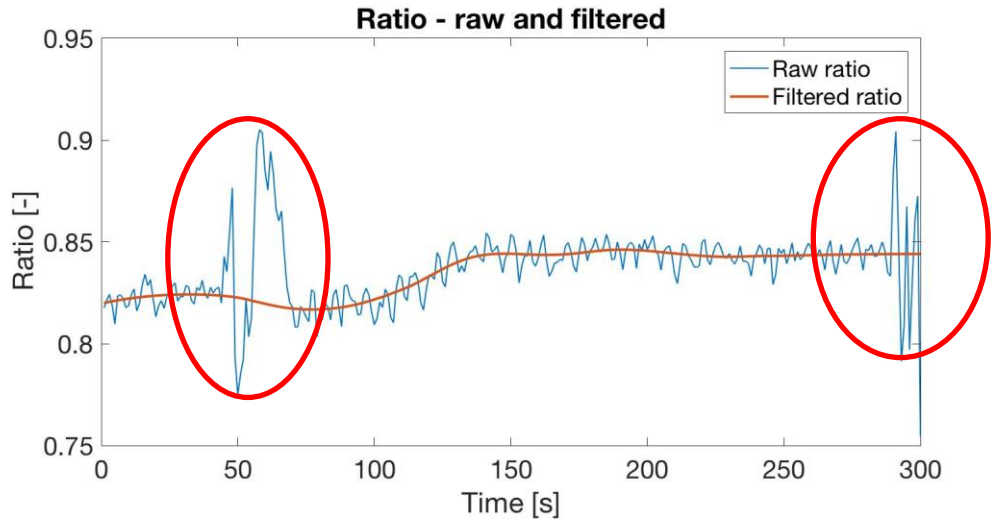

Figure 28: Ratio (IR, RED) - raw and filtered

Consequentially the blood oxygen saturation (SpO_2) can be evaluated for each value of the filtered ratio (see Listing 8: Calculation of the blood oxygen saturation). Figure 29 shows the trend of the blood oxygen saturation detected using the *Berry Pulse Oximeter BM1000C* device and the value of the developed prototype computed using the above-mentioned algorithm. It is possible to see that the results, despite a small offset (mean offset is equal to 9.67%), show good accordance.

Listing 8: Calculation of the blood oxygen saturation

```
for m = 1 : length (ratioFiltered)
   spo2(:,m)=110-25*ratioFiltered(m);
end
```

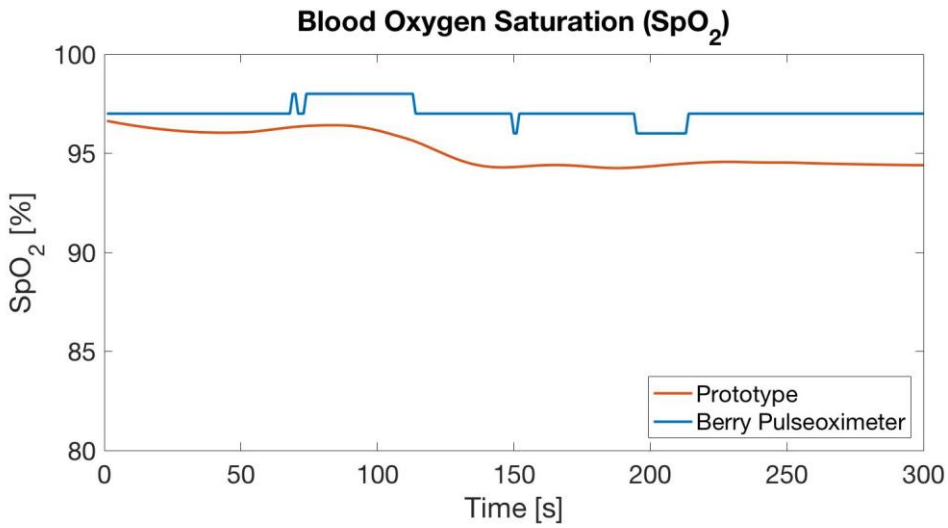

Figure 29: Blood oxygen saturation (SpO_2)

7 Results

This chapter portrays the resulting evaluation of the experimental setup described in chapter “6 Implementation, Testing”. Paragraph 7.1 describes errors of the peak detection for the PPG and ECG signals. Furthermore, the derived results for RR intervals as well as results for blood oxygen saturation values are consider and compared mentioning mean values as well as the standard deviation of each signal and subject.

7.1 Errors as not considered PPG peaks

As described in chapter “6.2.2 Algorithm for RR intervals evaluation” some detected peaks of the PPG signal had to be considered as errors on the basis of their distance threshold (30% of the average peak distance) to the corresponding ECG peak.

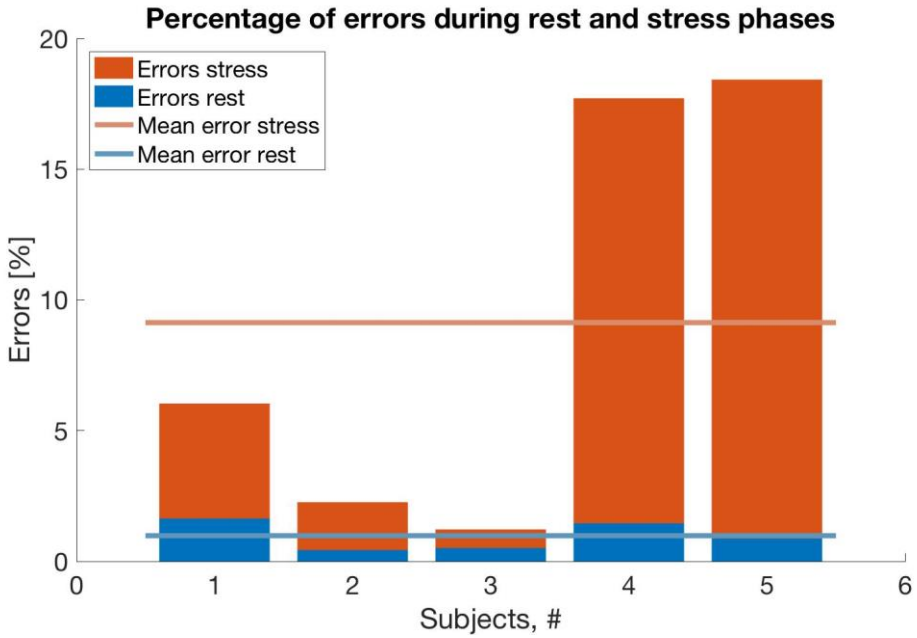

Figure 30: Absolute number of Errors in PPG peak detection for each subject during rest and stress phases

Figure 30 illustrates the percentage of errors (relative to the total number of detected ECG peaks) for each subject occurred during rest and stress phases. The blue line indicates the mean error value (0.868%) during rest while the red line

indicates the value for the mean error (6.034%) during stress. The mean value of errors significantly increases from rest (0.868%) to stress phases (6.034%).

7.2 RR intervals

The procedure described in chapter 6.2.1 has been applied to all the datasets and the results are listed in the following table (see Table 7: Summary of the results for the five subjects in rest (R) and stress (S) phases). For each subject, the mean value of all computed RR intervals as well as the standard deviation using ECG and PPG signals are listed.

Table 7: Summary of the results for the five subjects in rest (R) and stress (S) phases

Subject, #_phase	**Mean value, RR_{ECG}**	**Standard deviation, RR_{ECG}**	**Mean value, RR_{PPG}**	**Standard deviation, RR_{PPG}**
	[ms]	**[ms]**	**[ms]**	**[ms]**
1_R	758.18	52.525	758.17	55.468
2_R	641.56	15.761	641.54	16.880
3_R	649.42	41.767	649.40	43.113
4_R	978.19	29.621	978.13	31.295
5_R	872.09	61.817	872.39	65.936
1_S	603.88	24.043	603.81	25.441
2_S	481.99	47.169	481.86	53.548
3_S	574.65	23.136	575.79	42.402
4_S	644.49	52.904	644.72	63.519
5_S	672.16	27.809	671.30	46.836

The results show that the mean values for the RR intervals are lower during the stress phase than in the rest phase, as expected. The mean values computed with the PPG and the ECG signals are basically the same. The standard deviation is generally within ±10% of the mean value. The standard deviation value is higher

for the RR intervals evaluated using the PPG signal than the ones obtained using the ECG signal.

The following figure (Figure 31) represents the data listed in Table 7.

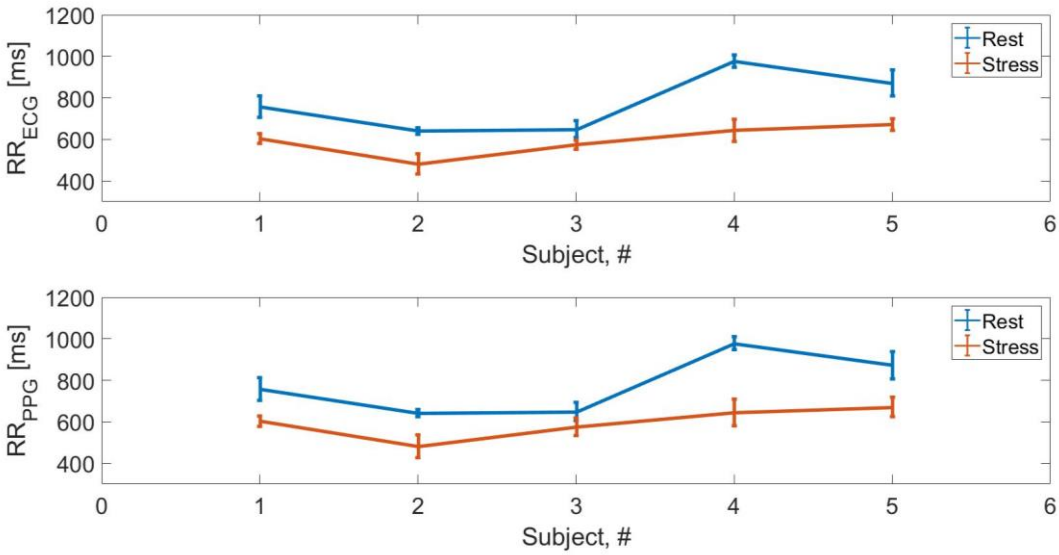

Figure 31: Mean values of RR intervals, evaluated using ECG and PPG signals with error bars

7.3 Blood oxygen saturation

The procedure described in chapter 6.2.2 has been applied to all the datasets and the results are listed in the following table (see Table 8: Summary of the results for the five subjects in rest (R) and stress (S) phases). For each subject, the mean value of all calculated SpO_2 values as well as the standard deviation using the PPG signal and the reference value of the *Berry Pulse Oximeter BM1000C* device are listed.

Table 8: Summary of the results for the five subjects in rest (R) and stress (S) phases

Subject, #_phase	**Mean value, $SpO_{2\ PPG}$**	**Standard deviation, $SpO_{2\ PPG}$**	**Mean value, $SpO_{2\ Berry}$**	**Standard deviation, $SpO_{2\ Berry}$**
	[%]	**[%]**	**[%]**	**[%]**
1_R	94	0.194	94	1.263
2_R	95	0.085	98	0.426
3_R	96	0.273	97	0.454
4_R	98	0.339	97	0.436
5_R	95	0.470	97	0.388
1_S	94	0.481	94	0.536
2_S	98	0.293	96	1.003
3_S	98	0.105	96	0.538
4_S	97	0.147	97	0.261
5_S	98	1.064	97	0.507

The results show that the general standard deviation values are lower using the PPG signal than the values derived by Berry©'s Pulse Oximeter. Furthermore, a higher standard deviation during the subjects' stress phase than during the rest phase can be observed.

Figure 32 represents the derived data of Table 8 for each subject using error bars.

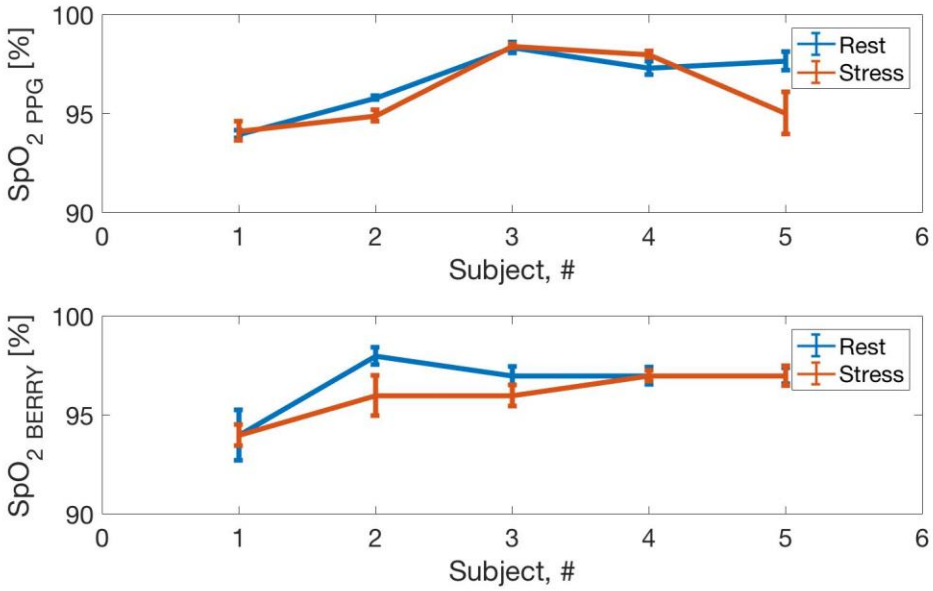

Figure 32: Mean values of blood oxygen saturation (SpO_2), evaluated using Berry©'s Pulse Oximeter and PPG signals with error bars

8 Bland-Altman and regression analysis

In the following sections, methods used for evaluating RR-intervals for both measurement systems are compared. The Bland-Altman analysis is proposed as a tool for the comparisons between the two methods.

Regarding blood oxygen saturation measurement methods, their limitations in the comparability of the results will be explained.

8.1 Comparison of RR-interval measurment methods

8.1.1 Introduction to Bland-Altman plots

Correlation quantifies the degree to which two variables are related. But a high correlation does not automatically imply that there is a good agreement between the two methods. The correlation coefficient and regression techniques are sometimes inadequate and can be misleading when assessing agreement, because they evaluate only the linear association of two sets of observations [45]

In 1983 Altman and Bland (B&A) proposed an alternative analysis, based on the quantification of the agreement between two quantitative measurements, by studying the mean difference and constructing limits of agreement [45]. These statistical limits are calculated by using the mean and the standard deviation (SD) of the differences between two measurements.

A graphical approach is used: the difference between the two paired measurements is plotted against the mean of the two measurements. Bland and Altman recommended that the 95% of the data points should lie within ± 1.96 SD of the mean difference.

The following figures (from Figure 33 to Figure 42) are the results of the comparisons of all the RR intervals evaluated using ECG and PPG signals. Each chart on the left side is the correlation plot, where the RR_{ECG} values are plotted versus the RR_{PPG} values. Each chart on the right side, is the Bland-Altman plot, where the differences between the results obtained using different devices are plotted versus the mean values of the two measurements. The symbols represent the data, while the lines correspond to the average value of the differences and the intervals of acceptability, namely ± 1.96 SD of the mean difference.

In general, a good agreement is obtained for the results related to the measurements performed during the rest phase, while during the stress phase the interval of acceptability is wider.

8.1.2 Regression & Bland-Altman plots during rest phase

As mentioned above, the results related to the measurements performed during rest phase show good agreement. The following five figures describe the evaluated results and are structured equally.

- On the left side, the regression plot of the two measurement methods is shown to statistically describe how strongly the pairs of RR-interval values are related. The x-axis of the regression plot characterizes the RR-intervals obtained by the ECG device while the y-axis represents corresponding RR-intervals measured by the PPG device. On the left upper side of the figures, the text-box gives additional information in regarding to: the equation of the regression line interpolating the data, the coefficient of determination (r^2), the sum of the squares of the errors (*SSE* [ms]) and the number of values considered in the analysis (*n*).
- On the right side, a Bland-Altman plot shows the agreement of the RR-interval measurements within a range of agreement, as described above in the introduction to the Bland-Altman plot.

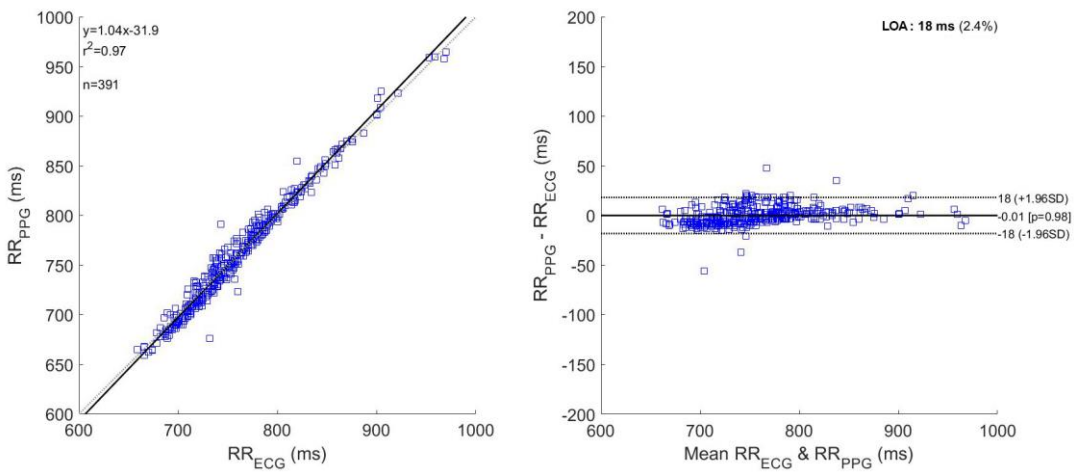

Figure 33: B&A plot – Subject 1 (Rest)

The measurements of the first subject (see Figure 33, left side) show a high correlation, namely a determination coefficient of r^2=*0.97*. The differences between the two measurements can be seen better in the Bland-Altman plot (see Figure 33, right side), which define as bias *-0.01 ms*, and an agreement range from *-18* to *+18* ms which is equal to *±1.96SD.* The limit of agreement is *18 ms*, while *2.4%* of values are not lying within the agreement range.

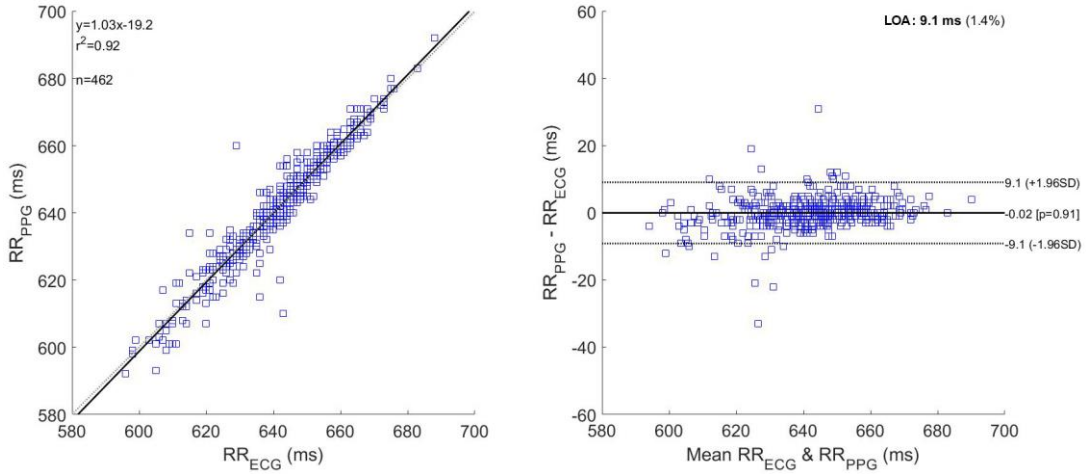

Figure 34: B&A plot – Subject 2 (Rest)

Figure 34 (left side) shows a determination coefficient of r^2=*0.92 for subject 2*. The Bland-Altman analysis of this subject shows the best result (see Figure 34, right), which define as bias *-0.02 ms*, and an agreement range from *-9.1* to *+9.1* ms equal to *±1.96SD.* The limit of agreement is *9.1 ms*, while *1.4%* of values are not lying within the agreement range.

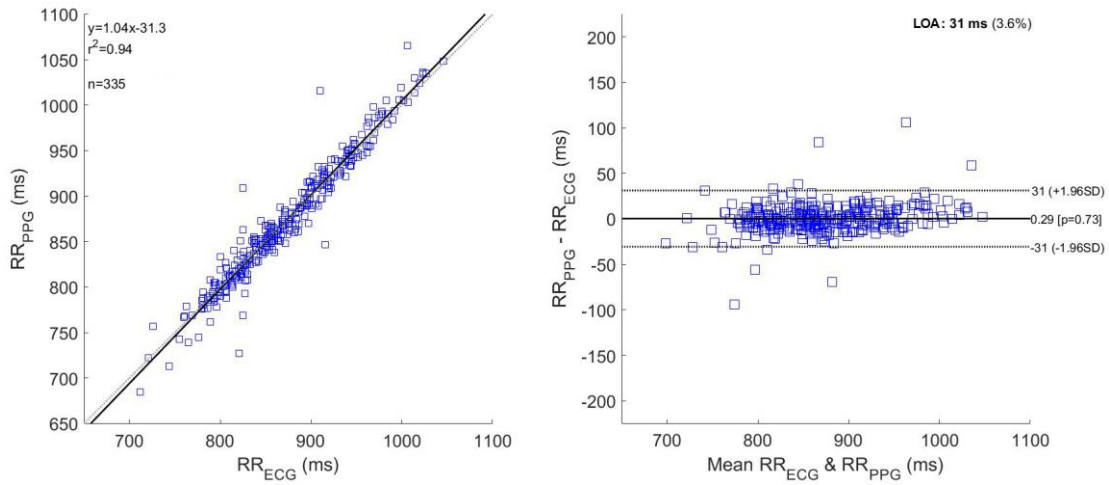

Figure 35: B&A plot – Subject 3 (Rest)

Figure 35 (left side) describes a determination coefficient of r^2=*0.92* for subject 3. The Bland-Altman analysis (see Figure 35, right) of this individual shows slightly higher bias of *0.29 ms*, and an agreement range from *-31* to *+31* ms equal to *±1.96SD.* The limit of agreement is *31 ms*, while *3.6%* of values are not lying within the agreement range.

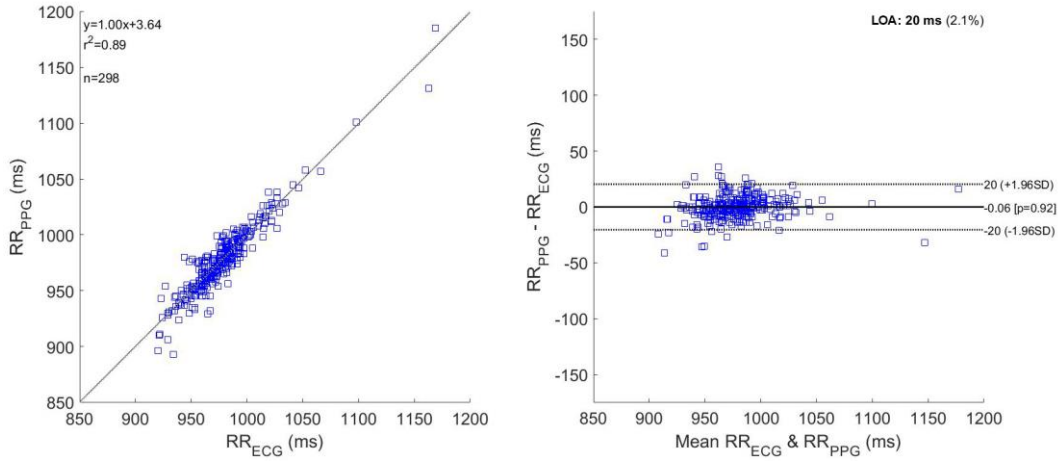

Figure 36: B&A plot – Subject 4 (Rest)

Figure 36 (left side) describes a lower determination coefficient of r^2=*0.89* for subject 3 compared to previous subjects. The Bland-Altman analysis (see Figure 36, right) of this individual shows a bias of *-0.06 ms*, and an agreement range from *-20* to *+20* ms equal to *±1.96SD.* Therefore, the limit of agreement is *20 ms*, while *2.1%* of values are not lying within the estimated agreement range.

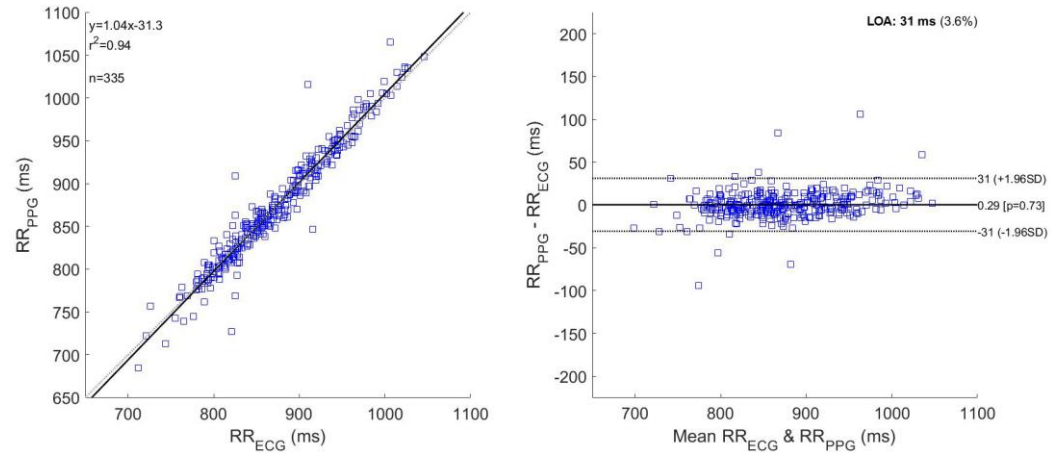

Figure 37: B&A plot – Subject 5 (Rest)

Figure 37 (left side) shows a determination coefficient of r^2=*0.94* for subject 5. The Bland-Altman analysis (see Figure 37, right) of this individual shows a bias of *0.29 ms*, and an agreement range from *-31* to *+31* ms equal to *±1.96SD.* Therefore, the limit of agreement is *31 ms*, while *3.6%* of values are not lying within the estimated agreement range.

8.1.3 Regression & Bland-Altman plots during stress phase

During stress phases the regression and Bland-Altman charts show generally lower results in the correlation of the derived RR-pairs as well as higher agreement range.

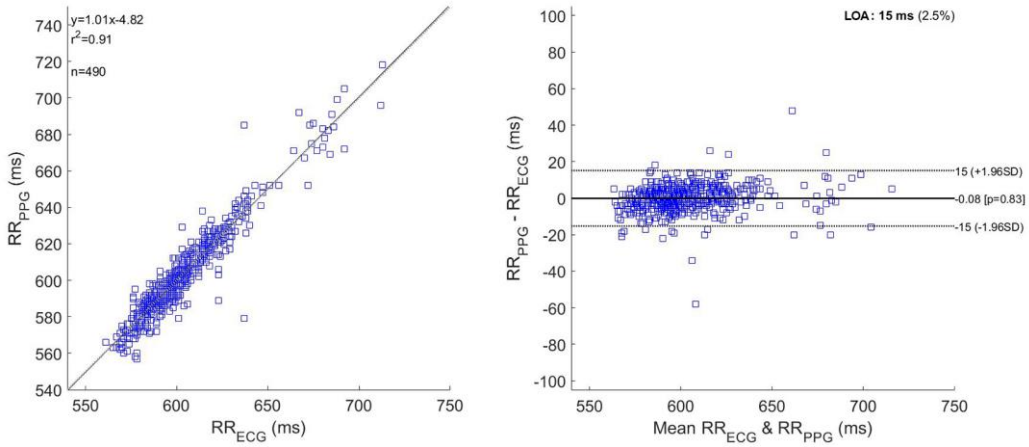

Figure 38: B&A plot – Subject 1 (Stress)

The measurements of the first subject (see Figure 38, left side) shows the highest correlation within the derived data during the stress phase, namely a determination coefficient of r^2=*0.97*. The Bland-Altman analysis of this subject (see Figure 38, right side), shows a bias *-0.08 ms*, and an agreement range from *-15* to *+15* ms, equal to *±1.96SD.* The limit of agreement is *15 ms*, while *2.5%* of values are not located within the agreement range.

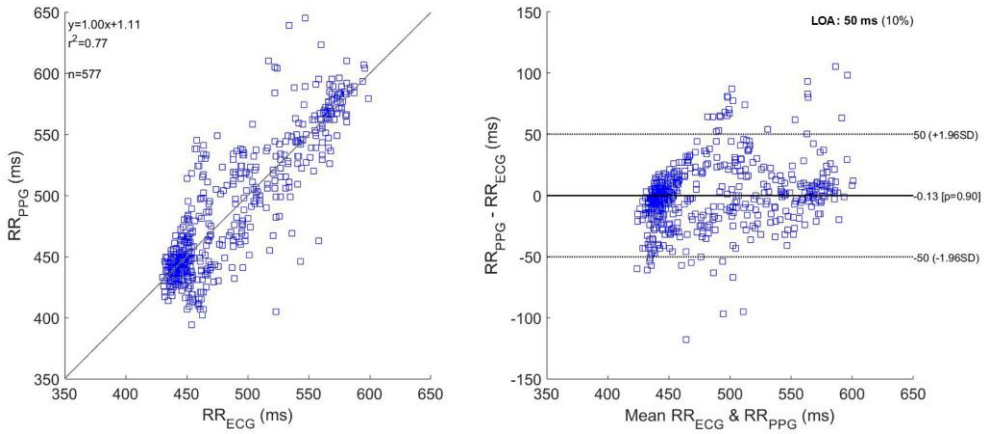

Figure 39: B&A plot – Subject 2 (Stress)

Figure 39 (left side) describes a determination coefficient of r^2=*0.92* for subject 2. The Bland-Altman analysis (see Figure 35, right) of this individual shows slightly higher bias of *0.29 ms*, and an agreement range from *-31* to *+31* ms equal to *±1.96SD.* The limit of agreement is *31 ms*, while *3.6%* of values are not located within the agreement range.

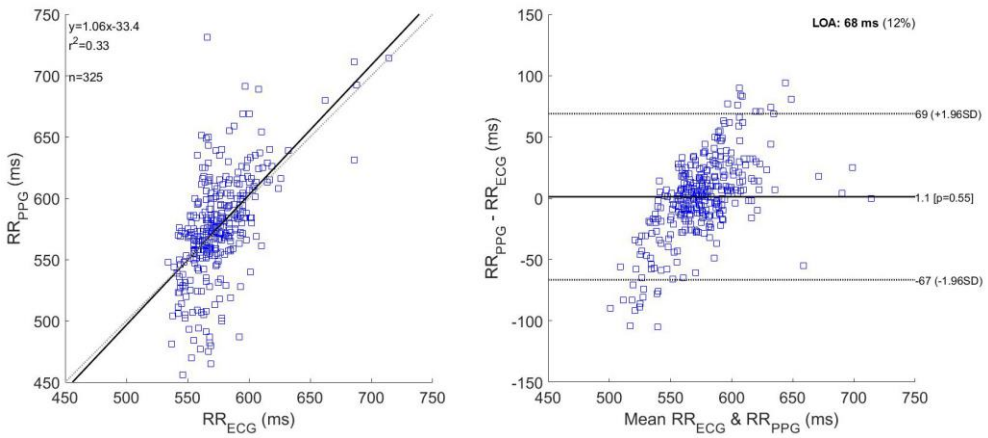

Figure 40: B&A plot – Subject 3 (Stress)

Figure 40 (left side) shows a determination coefficient of only r^2*=0.33 for subject 3*, which represents the lowest correlation compared to other subjects during stress phase. The Bland-Altman analysis of this individual (see Figure 40, right), which define as bias *-1.1 ms*, and an agreement range from *-69* to *+67* ms equal to *±1.96SD.* The limit of agreement is *68 ms*, while *12%* of values are not lying within the agreement range.

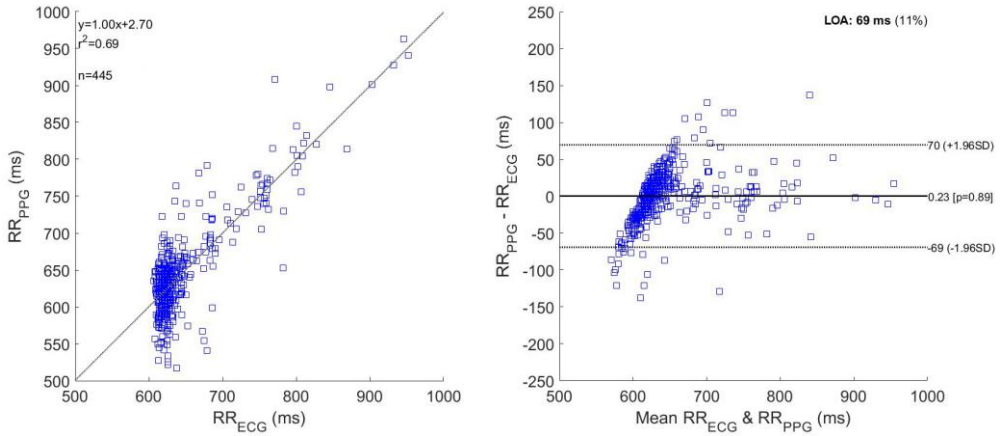

Figure 41: B&A plot – Subject 4 (Stress)

Figure 41 (left side) describes a determination coefficient of r^2*=0.69* for subject 4. The Bland-Altman analysis (see Figure 41, right) of this individual shows a bias of *0.23 ms*, and an agreement range from *-69* to *+70* ms equal to *±1.96SD.* Therefore, the limit of agreement is *69 ms*, while *11 %* of values are not located within the estimated agreement range.

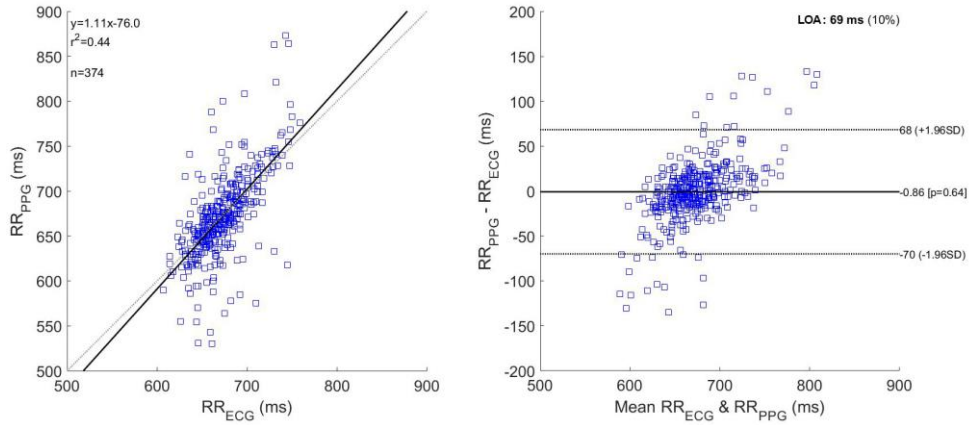

Figure 42: B&A plot – Subject 5 (Stress)

Figure 42 (left side) shows a determination coefficient of $r^2=0.44$ for subject 5. The Bland-Altman analysis (see Figure 37, right) of this individual shows a bias of *-0.86 ms*, and an agreement range from *-70* to *+68* ms equal to *±1.96SD.* Therefore, the limit of agreement is *69 ms*, while *10%* of values are not lying within the estimated agreement range.

8.1.4 Discussion of Bland-Altman and regression analysis

The following Table (see Table 9) shows a combined collection of the retrieved results from Bland-Altman and regression analysis for all five subjects during their rest phase.

Table 9: Collection of results of the Bland-Altman and regression analysis during rest phase

Subject, #_phase	Number of Samples	Bias	R2	LOA	Values outside LOA
	[-]	[ms]	[-]	[ms]	[%]
1_S	391	-0.01	0.97	18	2.4
2_S	462	-0.02	0.92	9.1	1.4
3_S	335	0.29	0.94	31	3.6
4_S	296	-0.06	0.89	20	2.1
5_S	335	0.29	0.94	31	3.6
Minimum	**296**	**-0.06**	**0.89**	**9.1**	**1.4**

Subject, #_phase	Number of Samples	Bias	R2	LOA	Values outside LOA
	[-]	[ms]	[-]	[ms]	[%]
Maximum	**462**	**0.29**	**0.97**	**31**	**3.6**
Average	**363.8**	**0.098**	**0.932**	**21.82**	**2.62**

The determination coefficient of the measurements varies from the lowest correlation r^2=0.89 to the highest of r^2=0.97. An average determination coefficient of r^2=0.94 indicates strong linear relationship between the two measurement methods of all subjects.

The limit of agreement (LOA) ranges from 9.1 to 31 ms, which means that at least 95% of the differences between ECG and PPG measurements are included within a range of 31ms. The average limit of agreement of 21.82 ms indicates a good agreement within all measurements during rest phases.

In contrast to the results during rest phases, the outcomes of Bland-Altman and regression analysis during stress phases show significant change. The results during stress phases are summarized in Table 10.

Table 10: Collection of results of the Bland-Altman and regression analysis during stress phase

Subject, #_phase	Number of Samples	Bias	R2	LOA	Values outside LOA
	[-]	[ms]	[-]	[ms]	[%]
1_S	490	-0.08	0.91	15	2.5
2_S	577	-0.13	0.77	50	10
3_S	325	1.1	0.33	68	12
4_S	445	0.23	0.69	69	5.5
5_S	374	-0.86	0.44	69	10
Minimum	**325**	**-0.86**	**0.33**	**15**	**2.5**
Maximum	**577**	**1.1**	**0.91**	**69**	**12**

Subject, #_phase	Number of Samples	Bias	R2	LOA	Values outside LOA
	[-]	[ms]	[-]	[ms]	[%]
Average	**442.2**	**0.052**	**0.628**	**54.2**	**8**

The determination coefficient of the measurements varies from the lowest correlation r^2=0.33 to the highest of r^2=0.91. An average determination coefficient of r^2=0.62 indicates a moderate relationship between the two measurement methods. Only the measurement methods of subject 1 show a strong linear relationship while those for subject 3 and 5 show a moderate to low linear correlation.

The limit of agreement (LOA) ranges from 15 to 69 ms. The average limit of agreement of 54.2 ms indicates a drastically increasing LOA value by the factor 2.48 compared to the average value of the results during rest. At the same time the average percentage of measurement values not included in the LOA range increases from 2.62% during rest phases to 8% during stress phases, which does not indicate good agreement of measurement methods. This result is also confirmed by the higher number for errors detected during stress phase, especially for the subjects 4 and 5, compared to the number of errors detected during the rest phase.

8.2 Comparison of blood oxygen saturation (SpO_2) measurement methods

Comparing the results of blood oxygen saturation of the prototype and the reference device (*Berry©'s Pulse Oximeter*), the following limitations of the comparability occurred:

- The reference device provided by Berry© has an accuracy of ±2% while delivering values for blood oxygen saturation [27].
- The used algorithm for calculating blood oxygen saturation results would need clinical calibration based on empirical data to a known standard before providing reliable results [2].
- Motion artefacts and light scattering, especially during subjects' stress phases can distort the results of both devices.

Therefore, Bland-Altman analysis as well as regression analysis are not used for statistical evaluation of each subject due to low correlation results. Despite of low correlation indices, the mean measurements of rest and stress phases seem to be reasonable to the physical blood oxygen saturation compared to the reference Pulse Oximeter. Figure 43 shows the regression plot (left) and the chart for Bland-Altman analysis (right) for the mean blood oxygen saturation values of each subject during rest and stress phases. The regression plot shows a moderate determination coefficient of r^2*=0.70.* The corresponding Bland-Altman analysis of shows a bias of *0.00%*, and an agreement range from *-1.8* to *+1.8* % equal to ±*1.96SD.* Therefore, the limit of agreement is *1.8 %*, while *1.9%* of values are not lying within the estimated agreement range which is below the accuracy limits of Berry©'s Pulse Oximeter (±2%).

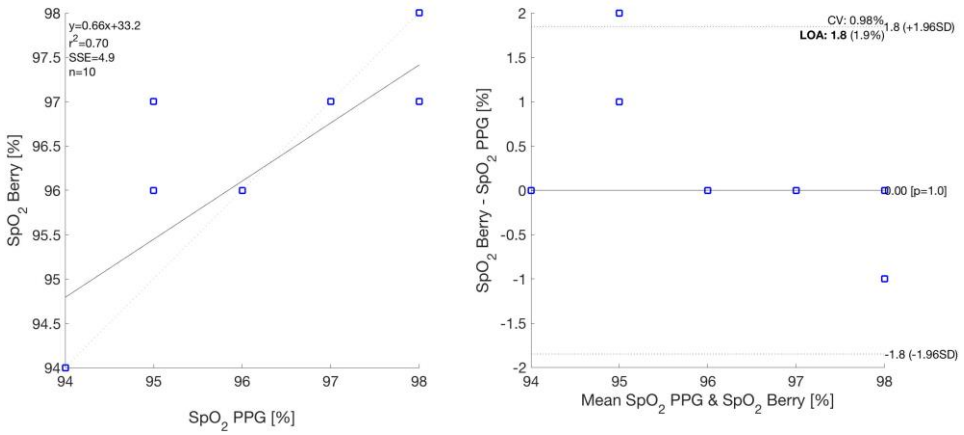

Figure 43: B&A plot of mean SpO_2 values of each subject in rest and stress phases

9 Conclusion

A low-cost prototype, fingertip reflective Bluetooth pulse oximeter using the method of photoplethysmography (PPG) was developed and evaluated to an electrocardiography device, considered as the golden standard for heart rate analysis. Five subjects' peak-to-peak intervals were tested during five minutes' rest (no physical exertion) and stress phases (moderate physical exertion).

The results showed suitable agreement between the present device and ECG-based device during rest phases (no physical exercise) phases. However, during phases of moderate physical exertion, the agreement between the mentioned devices dropped significantly by the average factor of 2.62. The results during stress phases showed moderate correlation and agreement.

The calculated peripheral blood oxygen saturation (SpO_2) during rest and stress phases showed a moderate agreement to a commercially available pulse oximeter, however for accurate results, the present device needs a clinical calibration based on a wide range of empirical data to a known standard.

Considering the relatively bad results of the developed device during phases of moderate physical exertion, further investigation especially in resolving motion artefacts cause by slight movements of the body during this phase are needed. Therefore, acceleration based motion artefacts reduction should be considered in works for future developed prototypes.

Literature

[1] A. C. Guyton, *Textbook of Medical Physiology 11th Eleventh Edition*, 111th, Eleventh Edition ed. Saunders Co., 2005.

[2] J. G. Webster, *Design of Pulse Oximeters*. Taylor & Francis Ltd, 1997.

[3] G. P. Rédei, Ed., "Electrocardiography," in *Encyclopedia of Genetics, Genomics, Proteomics and Informatics*, Dordrecht: Springer Netherlands, 2008, pp. 589–589.

[4] C. by Agateller, *Schematic diagram of normal sinus rhythm for a human heart as seen on ECG (with English labels).* 2007.

[5] User:Spl4, *English: A representative photoplethsmograph obtained from a Nonin pulse oximeter attached to the ear.* 2006.

[6] J. Allen, "Photoplethysmography and its application in clinical physiological measurement," *Physiol Meas*, vol. 28, no. 3, pp. R1-39, Mar. 2007.

[7] M. Abbod, Y.-R. Chiou, S.-H. Yang, S.-Z. Fan, and J.-S. Shieh, "Developing a monitoring psychological stress index system via photoplethysmography," *Artificial Life and Robotics*, vol. 16, no. 3, pp. 430–433, 2011.

[8] A. A. Kamal, J. B. Harness, G. Irving, and A. J. Mearns, "Skin photoplethysmography--a review," *Comput Methods Programs Biomed*, vol. 28, no. 4, pp. 257–269, Apr. 1989.

[9] K. A. Reddy, B. George, N. M. Mohan, and V. J. Kumar, "A Novel Calibration-Free Method of Measurement of Oxygen Saturation in Arterial Blood," *IEEE Transactions on Instrumentation and Measurement*, vol. 58, no. 5, pp. 1699–1705, May 2009.

[10] T. Tamura, Y. Maeda, M. Sekine, and M. Yoshida, "Wearable Photoplethysmographic Sensors—Past and Present," *Electronics*, vol. 3, no. 2, pp. 282–302, Apr. 2014.

[11] T. K. Lee and D. R. Westenskow, "Comparison of Blood Pressure Measured by Oscillometry from the Supraorbital Artery and Invasively from the Radial Artery," *Journal of Clinical Monitoring and Computing*, vol. 14, no. 2, pp. 113–117, 1998.

[12] A. A. Sepehri, A. Kocharian, A. Janani, and A. Gharehbaghi, "An Intelligent Phonocardiography for Automated Screening of Pediatric Heart Diseases," *Journal of Medical Systems*, vol. 40, no. 1, p. 16, 2015.

[13] M. Bolanos, H. Nazeran, and E. Haltiwanger, "Comparison of heart rate variability signal features derived from electrocardiography and photoplethysmography in healthy individuals," *Conf Proc IEEE Eng Med Biol Soc*, vol. 1, pp. 4289–4294, 2006.

[14] B. Makivić, M. D. Nikić, and M. S. Willis, "Heart Rate Variability (HRV) as a Tool for Diagnostic and Monitoring Performance in Sport and Physical Activities," *Journal of Exercise Physiology Online*, vol. 16, no. 3, pp. 103–131, 2013.

[15] F. V. A. Vasconcellos, A. Seabra, F. A. Cunha, R. A. Montenegro, E. Bouskela, and P. Farinatti, "Heart rate variability assessment with fingertip photoplethysmography and polar RS800cx as compared with electrocardiography in obese adolescents," *Blood Press Monit*, vol. 20, no. 6, pp. 351–360, Dec. 2015.

[16] A. A. Flatt and M. R. Esco, "Smartphone-Derived Heart-Rate Variability and Training Load in a Women's Soccer Team," *Int J Sports Physiol Perform*, vol. 10, no. 8, pp. 994–1000, Nov. 2015.

[17] A. E. Aubert, B. Seps, and F. Beckers, "Heart rate variability in athletes," *Sports Med*, vol. 33, no. 12, pp. 889–919, 2003.

[18] L. Schmitt *et al.*, “Typology of ‘Fatigue’ by Heart Rate Variability Analysis in Elite Nordic-skiers,” *Int J Sports Med*, vol. 36, no. 12, pp. 999–1007, Nov. 2015.
[19] G. Lu, F. Yang, J. A. Taylor, and J. F. Stein, “A comparison of photoplethysmography and ECG recording to analyse heart rate variability in healthy subjects,” *J Med Eng Technol*, vol. 33, no. 8, pp. 634–641, 2009.
[20] N. Selvaraj, A. Jaryal, J. Santhosh, K. K. Deepak, and S. Anand, “Assessment of heart rate variability derived from finger-tip photoplethysmography as compared to electrocardiography,” *J Med Eng Technol*, vol. 32, no. 6, pp. 479–484, Dec. 2008.
[21] “morpholio presents photoplethysmography technology transfer.” [Online]. Available: https://www.designboom.com/design/morpholio-photoplethysmography-technology-transfer-28-04-2014/. [Accessed: 28-Jul-2017].
[22] A. Shcherbina *et al.*, “Accuracy in Wrist-Worn, Sensor-Based Measurements of Heart Rate and Energy Expenditure in a Diverse Cohort,” *J Pers Med*, vol. 7, no. 2, May 2017.
[23] S. Lu *et al.*, “Can photoplethysmography variability serve as an alternative approach to obtain heart rate variability information?,” *J Clin Monit Comput*, vol. 22, no. 1, pp. 23–29, Feb. 2008.
[24] “Electrocardiography versus photoplethysmography in assessment of maternal heart rate variability during labor. - PubMed - NCBI.” [Online]. Available: https://www.ncbi.nlm.nih.gov/pubmed/27462527. [Accessed: 26-Jul-2017].
[25] M. Elgendi, I. Norton, M. Brearley, D. Abbott, and D. Schuurmans, “Systolic Peak Detection in Acceleration Photoplethysmograms Measured from Emergency Responders in Tropical Conditions,” *PLOS ONE*, vol. 8, no. 10, p. e76585, Oct. 2013.
[26] “Cooking Hacks - Electronic and IoT Kits, tutorials and guides for Makers and Education.” [Online]. Available: https://www.cooking-hacks.com/. [Accessed: 26-Jul-2017].
[27] “e-Health Sensor Platform Complete Kit V2.0 for Arduino, Raspberry Pi and Intel Galileo [Biometric / Medical Applications] - Now 4 Sensors available - Arduino - Shop.” [Online]. Available: https://www.cooking-hacks.com/ehealth-sensors-complete-kit-biometric-medical-arduino-raspberry-pi. [Accessed: 26-Jul-2017].
[28] “Pulse and Oxygen in Blood Sensor (SPO2) for e-Health Platform [Biometric / Medical Applications].” [Online]. Available: https://www.cooking-hacks.com/pulse-and-oxygen-in-blood-sensor-spo2-ehealth-medical. [Accessed: 26-Jul-2017].
[29] “China Digital Bluetooth Figertip Pulse Oximeter (BM1000C) Approved CE - China Oximeter, Fingertip Oximeter.” [Online]. Available: http://berrymedical.en.made-in-china.com/product/NBFmwGIDkrWs/China-Digital-Bluetooth-Figertip-Pulse-Oximeter-BM1000C-Approved-CE.html. [Accessed: 26-Jul-2017].
[30] “Pulse/Heartbeat Sensor | Modern Device.” [Online]. Available: https://moderndevice.com/product/pulse-heartbeat-sensor/. [Accessed: 17-Jan-2018].
[31] “D1 mini [WEMOS Electronics].” [Online]. Available: https://wiki.wemos.cc/products:d1:d1_mini#technical_specs. [Accessed: 07-Sep-2017].
[32] N. Kolban, *Kolban’s Book on the ESP32 & ESP8266*. Leanpub, 2015.
[33] “20 EN 1 KITS D1 mini Pro (V1.1.0) learning kit und MINI D1 (OLED summer micro SD BMP180 WS18B20 1 button DHT11 relais...) in 20 EN 1 KITS D1 mini Pro (V1.1.0) learning kit und MINI D1 (OLED summer micro SD BMP180

WS18B20 1-button DHT11 relais...) aus Ersatzteile auf AliExpress.com | Alibaba Group.” [Online]. Available: https://de.aliexpress.com/item/20-EN-1-KITS-WEMOS-D1-mini-Pro-V1-1-0-learning-kit-and-MINI-D1/32821248090.html. [Accessed: 11-Sep-2017].
[34] M. Ternek, “Game-based Health Monitoring using Tangible User Interface Objects,” Institut für Softwaretechnik und Interaktive Systeme, 2015.
[35] S. Reichelt *et al.*, “Development of an Implantable Pulse Oximeter,” *IEEE Transactions on Biomedical Engineering*, vol. 55, no. 2, pp. 581–588, Feb. 2008.
[36] P. K. Baheti and H. Garudadri, “An Ultra Low Power Pulse Oximeter Sensor Based on Compressed Sensing,” 2009, pp. 144–148.
[37] M. McEwen and K. Reynolds, “Noninvasive detection of bilirubin using pulsatile absorption,” *Australas Phys Eng Sci Med*, vol. 29, no. 1, pp. 78–83, Mar. 2006.
[38] “Gelled Self-adhesive Disposable Ag/AgCl - PLUX Store.” [Online]. Available: https://store.plux.info/electrodes/59-pre-gelled-self-adhesive-disposable-agagcl-eletrodes.html. [Accessed: 02-Jan-2018].
[39] “1-D data interpolation (table lookup) - MATLAB interp1 - MathWorks Deutschland.” [Online]. Available: https://de.mathworks.com/help/matlab/ref/interp1.html?searchHighlight=interp1&s_tid=doc_srchtitle. [Accessed: 02-Jan-2018].
[40] “Piecewise Cubic Hermite Interpolating Polynomial (PCHIP) - MATLAB pchip - MathWorks Deutschland.” [Online]. Available: https://de.mathworks.com/help/matlab/ref/pchip.html?s_tid=doc_ta. [Accessed: 02-Jan-2018].
[41] “Butterworth filter design - MATLAB butter - MathWorks Deutschland.” [Online]. Available: https://de.mathworks.com/help/signal/ref/butter.html?searchHighlight=butter&s_tid=doc_srchtitle. [Accessed: 02-Jan-2018].
[42] “Zero-phase digital filtering - MATLAB filtfilt - MathWorks Deutschland.” [Online]. Available: https://de.mathworks.com/help/signal/ref/filtfilt.html?searchHighlight=filtfilt&s_tid=doc_srchtitle. [Accessed: 02-Jan-2018].
[43] M. Elgendi, “On the Analysis of Fingertip Photoplethysmogram Signals,” *Curr Cardiol Rev*, vol. 8, no. 1, pp. 14–25, Feb. 2012.
[44] “Cross-correlation - MATLAB xcorr - MathWorks Deutschland.” [Online]. Available: https://de.mathworks.com/help/signal/ref/xcorr.html. [Accessed: 02-Jan-2018].
[45] D. Giavarina, “Understanding Bland Altman analysis,” *Biochem Med (Zagreb)*, vol. 25, no. 2, pp. 141–151, Jun. 2015.

List of Figures

List of Tables

Listings